

Co-Design of Unconventional Array Architectures and Antenna Elements for 5G Base Stations

G. Oliveri, *Senior Member, IEEE*, G. Gottardi, F. Robol, A. Polo, *Member, IEEE*, L. Poli, *Member, IEEE*, M. Salucci, *Member, IEEE*, M. Chuan, C. Massagrande, P. Vinetti, M. Mattivi, R. Lombardi, and A. Massa, *Senior Member, IEEE*

Abstract—An innovative methodological paradigm is proposed for the design of unconventional antenna systems for future 5G base stations. In such a *co-design* strategy, the antenna element (a spline-shaped patch embedded in a *finite array model*) and the overall irregularly clustered-array layout are simultaneously synthesized through a multi-objective antenna-shape-optimization combined with a sub-arrying technique based on a new single-objective integer-coded Genetic Algorithm able to intrinsically handle constraints on the cluster shapes/types. Selected numerical examples, drawn from an exhaustive design process, are presented to assess the advantages and the effectiveness of the proposed *co-design* scheme in view of the final manufacturing of 5G base stations thanks to its capability to take into account the impact of mutual coupling, non-ideal antenna patterns, and implementation limitations.

Index Terms—Clustered Arrays, Integer-coded Genetic Algorithm, 5G Radiating Systems, 5G Communications, Spline-shaped Patches, Multi-objective Optimization.

I. INTRODUCTION AND RATIONALE

THE FUTURE generation of mobile wireless technologies, commonly labeled as “5G”, is expected to deliver multi-gigabit-per-second data rates while minimizing costs, connection latencies, and power consumption [1][2][3]. To fit these requirements, significant advances with respect to previous-generation systems [2][4] are expected and required from the technological, the methodological, and the architectural viewpoints. This holds true even more for the radiating segment of 5G base stations [2][3][4][5]. Indeed, it is widely agreed [3] that 5G base station antennas will have to guarantee unprecedented level of flexibility and performance (i.e., supporting real-time adaptive beam reconfiguration/user tracking features and, possibly, enabling *MIMO* processing) to address the needs of next-generation mobile wireless systems in terms of data rates and network capacity [2]. Moreover,

Manuscript received December 0, 2016.

G. Oliveri, G. Gottardi, F. Robol, A. Polo, L. Poli, M. Salucci, and A. Massa are with the ELEDIA Research Center (ELEDIA@UniTN - University of Trento), Via Sommarive 9, Povo 38123 Trento - Italy (e-mail: {giacomo.oliveri, giorgio.gottardi, fabrizio.robol, alessandro.polo, lorenzo.poli, marco.salucci, andrea.massa}@unitn.it)

G. Oliveri and A. Massa are also with the ELEDIA Research Center (ELEDIA@L2S - UMR 8506), 3 rue Joliot Curie, 91192 Gif-sur-Yvette, France (e-mail: {giacomo.oliveri, andrea.massa}@l2s.centralesupelec.fr)

A. Massa is also with the ELEDIA Research Center (ELEDIA@UC3M - Universidad Carlos III de Madrid), Avenida de la Universidad 30, 28911 Leganes, Madrid - Spain (e-mail: andrea.massa@tsc.uc3m.es)

M. Chuan, C. Massagrande, P. Vinetti, M. Mattivi, and R. Lombardi are with Huawei Technologies, Palazzo Verrocchio 1, 20090 Segrate, Italy, (e-mail: {menchuan, claudio.massagrande, pietro.vinetti, maurizio.mattivi, renato.lombardi}@huawei.com)

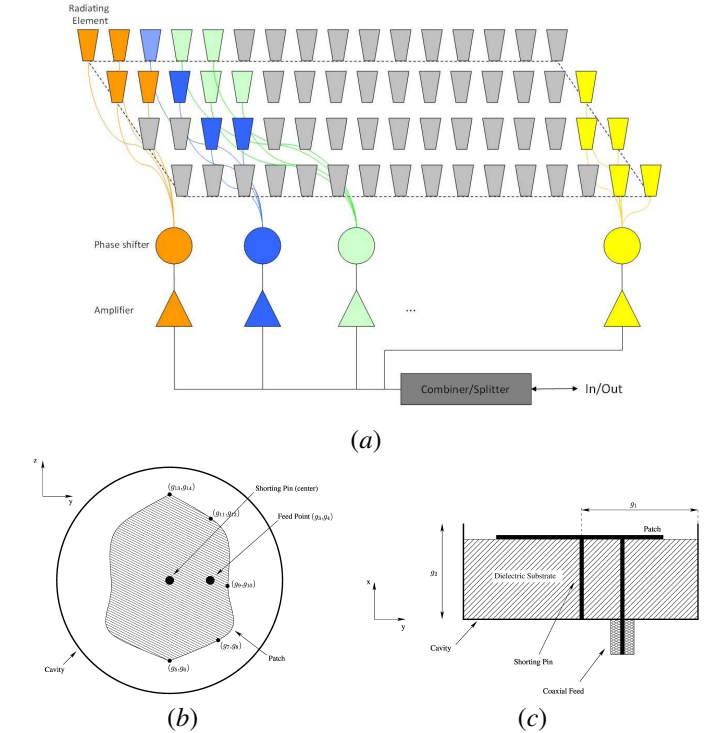


Figure 1. Reference 5G array architecture (a) and top-view (b) and side-view (c) of the elementary radiator.

these latter objectives will have to be obtained with inexpensive architectures and antenna elements to minimize the fabrication and the maintenance costs [2][3][4][5]. Therefore, it will not be possible to adopt for future 5G scenarios the traditional/conventional antenna solutions developed for the current generation base stations and conceived to exhibit a fixed beam covering the entire 120 [deg] “cellular sector” [2]. Active electronically scanned arrays (AESAs) [6][7] are a promising technology to address 5G base station antenna design [3][8][9][10][11][12]. Indeed, AESAs can exhibit real-time beam control, low sidelobes, high gain, narrow beamwidth, wide steering angle, wide bandwidth, as well as *MIMO* capabilities [6][7]. Unfortunately, jointly fitting all these requirements is very challenging especially if inexpensive (i.e., comprising few control points) and compact arrangements are required [10][11]. Generally speaking, popular AESA architectures such as (i) fully-populated (ideally enabling full pattern control/reconfiguration) and (ii) regularly

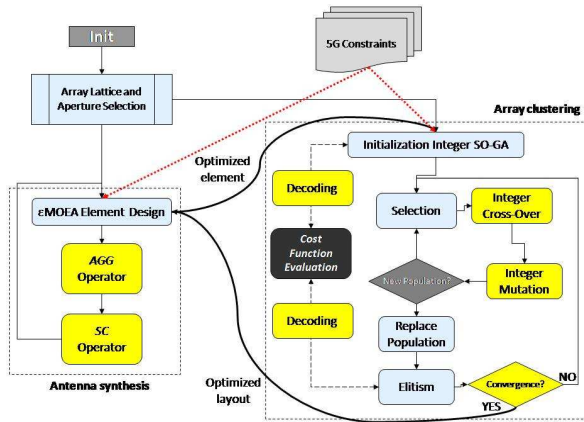


Figure 2. Flowchart of the proposed co-design strategy (yellow boxes highlight *ad-hoc* customized operators).

clustered layouts (featuring simplified feed networks comprising only few phase shifters/magnitude controls) cannot be adopted because of the high costs or the very limited field-of-view (not compliant with the 120 [deg] coverage angle required by cellular base stations), respectively [6][7]. Moreover, the design of the elementary radiator in the AESA cannot be carried out with standard approaches owing to the peculiar features of the 5G scenario in terms of number of constraints (yielding to a *massive-multi-objective [MMO]* design problem) and type of objectives/requirements (e.g., an element isolation suitable for *MIMO* capabilities; a bandwidth enabling high data rates; a beamwidth for a satisfactory cellular sector coverage, etc ...) [13][14] to be satisfied when the antenna is *embedded* in the finite array system (i.e., not in a *stand-alone* or *periodic* configuration). Consequently, “atypical” solutions in terms of radiating system features and design strategies are mandatory to properly address the synthesis of 5G antenna systems.

In such a framework, an innovative method is here described for the synthesis of radiating systems for future 5G base stations. It is based on a *co-design* process in which the antenna element, embedded in the *finite* layout, and the array architecture (i.e., the radiators displacement and their feedings) are simultaneously synthesized by taking into account real-systems impact. Indeed, the proposed strategy is aimed at effectively handling the interrelationships arising in the 5G scenario between the single radiator and the array architecture since (i) the array geometry directly modifies the mutual coupling effects among the antenna elements that affect the 5G figures-of-merit of the single array element (e.g., the impedance, the isolation, and the radiation pattern) and, in turn, (ii) the antenna response (e.g., the beamwidth and the pattern slope) impacts the sidelobe control and the steering features of the resulting array layout. More specifically, such a *co-design* technique aims at synthesizing an *unconventional* array architecture [6][15] featuring *irregularly* clustered excitations [Fig. 1(a)] coupled with an elementary antenna consisting of a cavity-backed planar patch structure with a spline-based contour [16][17] [Fig. 1(b)]. Such architectural choices, which

yield to the derivation of completely new designs both for the array and for the elementary radiator with respect to traditional solutions [2], mainly derive from the 5G guidelines and they are motivated by the following:

- irregularly clustered arrangements potentially enable a significant mitigation of the feed network complexity (i.e., a reduction of the number of control points) with respect to fully-populated layouts while also allowing a moderation of the phase quantization lobes usually appearing in regular sub-arrayed systems when steered [6][15];
- the combination of spline-contoured patch antennas [16][17] with cavity backing is expected to enable a wide flexibility (when compared to standard geometries [16][17]) to address the 5G *MMO* problem as well as to allow a low inter-element coupling with technologically simple and quite inexpensive structures.

Despite such promising features, the design of the system now at hand is still very challenging task since, to the best of the authors’ knowledge, (a) no methodologies exist that allow the control of the sidelobe profile of sub-arrayed layouts over wide scanning angles and bandwidths when the excitation magnitudes and phases are jointly clustered¹ and (ii) spline-contoured patches have never been designed in a 5G *MMO* scenario by taking into account their interactions with the surrounding elements in view of the reliable base station prototyping [16][17]².

To address such challenges, the proposed *co-design* procedure exploits the combination of

- an innovative *irregular* clustering technique that formulates the sub-arrying problem as a global optimization one where the degrees-of-freedom (*DoFs*) are the clustering scheme (i.e., the suitable combination of a set of admissible *a-priori* chosen “shapes/tiles”) and the cluster excitations, while the cost function encodes the compliancy of the synthesized pattern with the 5G sidelobe mask defined for all steering angles and within the whole operative frequency band;

and

- a customized shape-optimization aimed at defining, through a suitable *multi-objective* search [21][22], a radiating element that meets the 5G electrical requirements (i.e, input impedance, beamwidth, isolation, polarization, etc) when embedded in a finite array and not alone or in an infinite periodic arrangement as usually done in the state-of-the-art literature.

Following the “No-free-lunch” Theorem [23], *ad-hoc* search strategies are selected to efficiently address the above 5G design sub-problems. More specifically, (a) a single-objective

¹Such feeding architecture is employed only for very limited scan angles/bands by state-of-the-art approaches [7][18], while more complex arrangements comprising many more phase shifters than magnitude controls are adopted if wider fields-of-view (such as those of interest in 5G) are required [6][19][20].

²Conventional spline-contoured antennas have been proposed only for stand-alone applications and considering single-objective design strategies [16][17].

Genetic Algorithm (*SO-GA*) [24][25][26] featuring an innovative integer coding of the variables and *ad-hoc* operators for handling the irregular clustering, while (b) the *MMO* shaped-optimization of the elementary radiator is carried out after a suitable reformulation through a ε -*MOEA* approach [21][22]. In summary, the main innovative methodological contributions of this work include (i) the introduction of an innovative *co-design* technique addressing the synthesis of both the array layout and the elementary radiator geometry for *unconventional* architectures, (ii) the development of a new integer-coded *GA* clustering methodology able to *a-priori* intrinsically handle constraints on the technologically admissible sub-array shapes, (iii) the derivation of a multi-objective formulation for the *MMO* 5G antenna design in which the array element is synthesized by means of an ε -*MOEA* technique to take into account the real impact of the surrounding radiators without relying on “*stand-alone*” or “*periodic*” approximated models, (iv) the derivation of a set of applicative guidelines on the potentialities and the limitations of unconventional architectures in 5G base stations, and (v) the design of new *unconventional* arrangements (i.e., *irregularly* clustered but employing modular sub-arrays) to reduce quantization lobes over wide steering angles while mitigating their complexity and costs [6] and new *unconventional* radiators (i.e., cavity-backed *spline-contoured* geometries) able to simultaneously meet the multiple and contrasting 5G guidelines when embedded in a finite array.

The paper is organized as follows. The 5G base station design problem is formulated in Sect. II. In Sect. III, the proposed *co-design* methodology is introduced and detailed. Representative synthesis examples drawn from real and on-going projects are presented next (Sect. IV) to illustrate the features of the proposed approach as well as to prove its effectiveness in taking into account the impact of mutual coupling, non-ideal antenna patterns, and implementation limitations on the performance of 5G unconventional architectures. Conclusions and final remarks will follow (Sect. V).

II. 5G BASE STATION ANTENNA DESIGN PROBLEM

With reference to the architectural choices devised in Sect. I, let us consider a planar arrangement of N elements displaced in the yz -plane [Fig. 1(a)] and clustered in Q sub-arrays of contiguous elements as indicated by the membership vector $\mathbf{s} \triangleq \{s_n \in [0, Q-1]; n = 1, \dots, N\}$, whose n -th entry $s_n = q$ indicates the membership of the n -th array element to the q -th cluster. Since all the elements of the q -th cluster are fed with the same excitation magnitude, a_q , and phase, $\psi_q(\theta_0, \varphi_0; f)$, which depends on the steering angle (θ_0, φ_0) and the working frequency f , the far-field power pattern radiated by the array is given by [6][7]

$$\mathcal{P}(\theta, \varphi; \theta_0, \varphi_0; f) = \left| \sum_{q=0}^{Q-1} \left\{ a_q \exp[j\psi_q(\theta_0, \varphi_0; f)] \right. \right. \\ \left. \left. \sum_{n=0}^{N-1} \delta_{qs_n} E_n(\theta, \varphi; f) \exp(j\frac{2\pi}{\lambda} \mathbf{r}_n \cdot \hat{\mathbf{r}}) \right\} \right|^2 \quad (1)$$

where λ is the wavelength at f , δ_{qs_n} is the Kronecker delta function ($\delta_{qs_n} = 1$ if $s_n = q$ and $\delta_{qs_n} = 0$ otherwise), and

$$\hat{\mathbf{r}} = \sin(\theta) \sin(\varphi) \hat{\mathbf{y}} + \cos(\theta) \hat{\mathbf{z}}. \quad (2)$$

Moreover, $\mathbf{r}_n = y_n \hat{\mathbf{y}} + z_n \hat{\mathbf{z}}$ is the position of the n -th ($n = 1, \dots, N$) array element, while $E_n(\theta, \varphi; f)$ is the corresponding radiation pattern, which is a function of the M -size vector of its geometrical descriptors [Fig. 1(b)]

$$\mathbf{g} \triangleq \{g_m, m = 1, \dots, M\}. \quad (3)$$

To design a 5G base station antenna, manifold objectives/requirements pertaining the array pattern (i.e., sidelobe mask compliancy for all the steering angles and within the whole frequency band of interest) and the array element radiation features (i.e., impedance matching, isolation from surrounding elements, polarization ellipticity, gain, and beamwidth) must be fitted [3][13][11]³. As a result, the synthesis at hand turns out to inherently be a *MMO* problem when formulated as that of the optimal setup of the unknown vectors $\{\mathbf{s}, \mathbf{a} \triangleq \{a_q, q = 1, \dots, Q\}, \Psi, \mathbf{g}\}$ such that

$$\{\mathbf{s}, \mathbf{a}, \Psi, \mathbf{g}\}^{opt} = \arg \min_{\{\mathbf{s}, \mathbf{a}, \Psi, \mathbf{g}\}} [\Phi(\mathbf{s}, \mathbf{a}, \Psi, \mathbf{g})] \quad (4)$$

where

$$\Psi \triangleq \{\psi_q(\theta_0, \varphi_0; f); q = 1, \dots, Q; \theta_0 \in [\theta_0^{\min}, \theta_0^{\max}], \varphi_0 \in [\varphi_0^{\min}, \varphi_0^{\max}], f \in [f^{\min}, f^{\max}]\} \quad (5)$$

is the set of excitation phases of the Q clusters in the ranges $f \in [f^{\min}, f^{\max}]$, $\theta_0 \in [\theta_0^{\min}, \theta_0^{\max}]$, and $\varphi_0 \in [\varphi_0^{\min}, \varphi_0^{\max}]$ of the 5G requirements. Moreover,

$$\Phi(\mathbf{s}, \mathbf{a}, \Psi, \mathbf{g}) \triangleq \{\Phi_l(\mathbf{s}, \mathbf{a}, \Psi, \mathbf{g}), l = 1, \dots, L\} \quad (6)$$

is the *MMO* cost function set comprising L terms encoding the synthesis objectives as follows⁴:

- “*Array Sidelobe Mask Compliancy*” Term ($l = 1$):

$$\Phi_1(\mathbf{s}, \mathbf{a}, \Psi, \mathbf{g}) \triangleq \frac{1}{(f^{\max} - f^{\min})(\varphi_0^{\max} - \varphi_0^{\min})(\theta_0^{\max} - \theta_0^{\min})} \times \\ \times \int_{f^{\min}}^{f^{\max}} \int_{\theta_0^{\min}}^{\theta_0^{\max}} \int_{\varphi_0^{\min}}^{\varphi_0^{\max}} \max_{\theta, \varphi} \{ \mathcal{R}[\mathcal{P}(\theta, \varphi; \theta_0, \varphi_0; f) - \mathcal{P}^T(\theta, \varphi; \theta_0, \varphi_0; f)] \} d\theta_0 d\varphi_0 df \quad (7)$$

where $\mathcal{P}^T(\theta, \varphi; \theta_0, \varphi_0)$ is the target sidelobe when the array is steered towards (θ_0, φ_0) and $\mathcal{R}[\cdot]$ is the “ramp” function ($\mathcal{R}[\cdot] \triangleq [\cdot] \times \mathcal{H}[\cdot]$, $\mathcal{H}[\cdot]$ being the Heaviside function);

- “*Element Impedance Matching*” Term ($l = 2$):

$$\Phi_2(\mathbf{s}, \mathbf{a}, \Psi, \mathbf{g}) = \\ = \Phi_2(\mathbf{s}, \mathbf{g}) \triangleq \frac{\int_{f^{\min}}^{f^{\max}} \mathcal{R}[|\mathcal{S}_{11}(f)| - |\mathcal{S}_{11}^T(f)|] df}{(f^{\max} - f^{\min})} \quad (8)$$

where $\mathcal{S}_{11}(f)$ and \mathcal{S}_{11}^T are the synthesized and the target antenna reflection coefficient at the input port at the frequency f , respectively;

³Although 5G standards have not yet been officially published, a set of frequency bands have already been released [27], and guidelines regarding the envisaged performance and indicators to be optimized for 3D beamforming, active antenna, and massive MIMO systems have already been discussed [3][13][11][28]. Moreover, owing to its full generality, the proposed *co-design* strategy will be seamlessly exploitable/customizable when the 5G official requirements will be released.

⁴For the sake of notation compactness, the dependency of all the radiation quantities (i.e., pattern, gain, sidelobe, reflection coefficient, etc.) on the *DoFs* vector ($\mathbf{s}, \mathbf{a}, \Psi, \mathbf{g}$) is omitted hereinafter.

- “Element Polarization” Term ($l = 3$):

$$\Phi_3(\mathbf{s}, \mathbf{a}, \Psi, \mathbf{g}) = \Phi_3(\mathbf{s}, \mathbf{g}) \triangleq \frac{\int_{f^{\min}}^{f^{\max}} [\varepsilon(f) - \varepsilon^T]^2 df}{(f^{\max} - f^{\min})}$$

where $\varepsilon(f)$ and ε^T are the synthesized and the target antenna polarization ellipticity angle at the frequency f , respectively;

- “Element Beamwidth” Terms ($l = 4, 5$):

$$\left\{ \begin{array}{l} \Phi_4(\mathbf{s}, \mathbf{a}, \Psi, \mathbf{g}) = \\ = \Phi_4(\mathbf{s}, \mathbf{g}) \triangleq \frac{\int_{f^{\min}}^{f^{\max}} \mathcal{R}[W_{AZ}(f) - W_{AZ}^T] df}{(f^{\max} - f^{\min})} \\ \Phi_5(\mathbf{s}, \mathbf{a}, \Psi, \mathbf{g}) = \\ = \Phi_5(\mathbf{s}, \mathbf{g}) \triangleq \frac{\int_{f^{\min}}^{f^{\max}} \mathcal{R}[W_{EL}(f) - W_{EL}^T] df}{(f^{\max} - f^{\min})} \end{array} \right. \quad (9)$$

where $W_{AZ}(f) = \left| \arg \min_{\varphi \in [0, \varphi_M]} \left| \frac{E(\theta_M, \varphi; f)}{E(\theta_M, \varphi_M; f)} - 0.5 \right| - \arg \min_{\varphi \in [-\frac{\pi}{2}, \varphi_M]} \left| \frac{E(\theta_M, \varphi; f)}{E(\theta_M, \varphi_M; f)} - 0.5 \right| \right|$ and $W_{EL}(f) = \left| \arg \min_{\theta \in [\theta_M, \pi]} \left| \frac{E(\theta, \varphi_M; f)}{E(\theta_M, \varphi_M; f)} - 0.5 \right| - \arg \min_{\theta \in [0, \theta_M]} \left| \frac{E(\theta, \varphi_M; f)}{E(\theta_M, \varphi_M; f)} - 0.5 \right| \right|$ are the antenna half-power beamwidths in azimuth and elevation, while W_{AZ}^T and W_{EL}^T the corresponding target values, being $(\theta_M = \frac{\pi}{2}, \varphi_M = 0)$ the element broadside direction, and $E(\theta, \varphi; f) = \frac{1}{N} \sum_{n=0}^{N-1} E_n(\theta, \varphi; f)$ is the average element factor;

- “Element Realized Gain” Term ($l = 6$):

$$\Phi_6(\mathbf{s}, \mathbf{a}, \Psi, \mathbf{g}) \triangleq \\ = \frac{\int_{f^{\min}}^{f^{\max}} \mathcal{R} \left[G^T - \frac{4\pi\kappa_1(f)\kappa_2(f)E(\theta_M, \varphi_M; f)}{J_0^2\pi \int_0^\pi [E(\theta, \varphi; f) \sin(\theta)] d\theta d\varphi} \right] df}{(f^{\max} - f^{\min})} \quad (10)$$

where G^T is the target realized gain value, while $\kappa_1(f)$ and $\kappa_2(f)$ are the average element efficiency and the average mismatch factor, respectively;

- “Element Isolation” terms ($l = 7, \dots, L$):

$$\Phi_l(\mathbf{s}, \mathbf{a}, \Psi, \mathbf{g}) \triangleq \\ = \frac{\int_{f^{\min}}^{f^{\max}} \mathcal{R} [|\mathcal{S}_{k1}(f)| - |\mathcal{S}_{k1}^T|] df}{(f^{\max} - f^{\min})} \quad k = l - 6; l = 7, \dots, L \quad (11)$$

where $\mathcal{S}_{k1}(f)$ and \mathcal{S}_{k1}^T are the synthesized and the target isolation coefficients between the reference antenna and its k -th neighbor element at the frequency f , respectively.

Since solving the *MMO* problem in (4) with a single step procedure is not feasible because of the unavailability of effective and efficient *MO* optimization strategies when $L \geq 4$, the complex and highly non-linear nature of the objective functions/terms in (6), and the large number of *DoFs*, $\{\mathbf{s}, \mathbf{a}, \Psi, \mathbf{g}\}$, resulting in a too huge and computationally untractable search space, it has been split into two (still connected) simpler ones concerned with (i) the array design and (ii) the element synthesis. Namely,

- a *single-objective (SO)* array clustering problem where the *DoFs* comprise the clustering scheme \mathbf{s} and the excitation vectors \mathbf{a} and Ψ , the *SO* cost function being defined, for a fixed radiator geometry ($\mathbf{g} = \bar{\mathbf{g}}$), as follows

$$\Phi_{SO}(\mathbf{s}, \mathbf{a}, \Psi) \triangleq \Phi_1(\mathbf{s}, \mathbf{a}, \Psi, \bar{\mathbf{g}}); \quad (12)$$

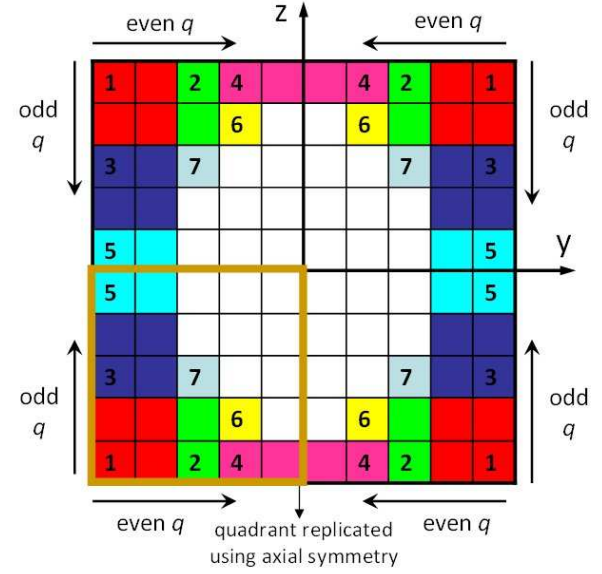


Figure 3. Sketch of the integer-coded *SO-GA* decoding technique for cluster placement.

- a *MMO* radiating element design problem where the *DoFs* are the geometry parameters \mathbf{g} , while the *MMO* cost function, for a fixed set of the remaining parameters $(\{\bar{\mathbf{s}}, \bar{\mathbf{a}}, \bar{\Psi}\})$, is given by

$$\Phi_{MMO}(\mathbf{g}) \triangleq \{\Phi_l(\bar{\mathbf{s}}, \bar{\mathbf{a}}, \bar{\Psi}, \mathbf{g}); l = 2, \dots, L\}. \quad (13)$$

It is worth remarking that (12) and (13) are generally tightly coupled problems, but even more in the *5G* scenario.

III. Co-Design SYNTHESIS STRATEGY

Because of the coupled nature of the problems formulated in Sect. II, an *alternate two-step co-design* process (Sect. III-C) is considered by first optimizing the cost function Φ_{SO} (12) when $\mathbf{g} = \bar{\mathbf{g}}$ (“*Array Clustering*” Phase - Sect. III-C) and then (“*Antenna Element Synthesis*” Phase - Sect. III-C) Φ_{MMO} (13) is minimized for a fixed *DoFs* configuration $\{\bar{\mathbf{s}}, \bar{\mathbf{a}}, \bar{\Psi}\}$ (Fig. 2).

A. “Array Clustering” Step (Integer-Coded SO-GA)

In order to properly address the *SO* problem (12) of the “*Array Clustering*” step, let us first notice that, for a given membership vector \mathbf{s} and a fixed setup of \mathbf{g} ($\mathbf{g} = \bar{\mathbf{g}}$), the optimal values of the array excitations in both amplitude, \mathbf{a} , and phase, Ψ , for a user-specified frequency f ($f \in [f^{\min}, f^{\max}]$) and a steering direction (θ_0, φ_0) ($\theta_0 \in [\theta_0^{\min}, \theta_0^{\max}]$, $\varphi_0 \in [\varphi_0^{\min}, \varphi_0^{\max}]$), are unique and they can be found by solving the following convex problem [29]

$$[\mathbf{a}(\mathbf{s}), \Psi(\theta_0, \varphi_0; f; \mathbf{s})]^{opt} \triangleq \\ = \arg \min_{\mathbf{a}(\mathbf{s}), \Psi(\theta_0, \varphi_0; f; \mathbf{s})} [D(\theta_0, \varphi_0; f)]^{-1} \quad (14) \\ s.t \mathcal{P}(\theta, \varphi; \theta_0, \varphi_0; f) \leq \mathcal{P}^T(\theta, \varphi; \theta_0, \varphi_0; f)$$

where $D(\theta_0, \varphi_0; f) = \frac{4\pi \mathcal{P}(\theta, \varphi; \theta_0, \varphi_0; f)}{\int_0^\pi \int_0^{2\pi} [\mathcal{P}(\theta, \varphi; \theta_0, \varphi_0; f) \sin(\theta)] d\theta d\varphi}$ is the array directivity. Indeed,

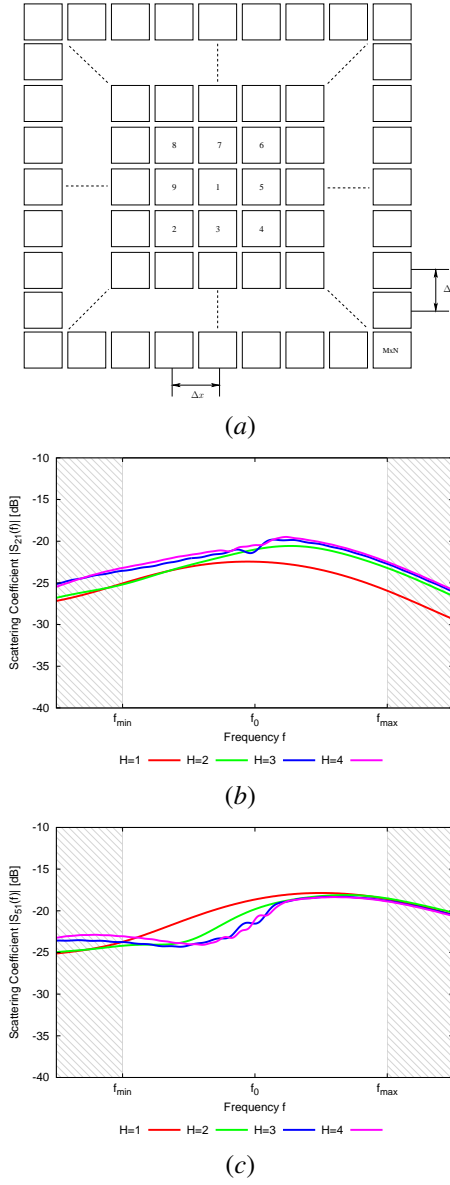


Figure 4. Calibration (Rectangular lattice, $0.492\lambda_0 \times 0.651\lambda_0$ unit cell) - Extended finite model (a) and behaviour of $|S_{k1}(f)|$ versus frequency when varying the number of rings H surrounding the reference antenna when (b) $k = 2$ and (c) $k = 5$.

$\Phi_{SO} \left([\mathbf{a}(\mathbf{s}), \boldsymbol{\psi}(\theta_0, \varphi_0; f; \mathbf{s})]^{opt} \right) = 0$. Accordingly, since the solution of the convex problem (14) is unique and it can be found with state-of-the-art convex programming tools [29], it turns out that the DoFs of the Array Clustering phase are only the memberships of the array elements listed in the integer membership vector \mathbf{s} and the optimization problem at hand can be classified as a *SO discrete* one.

As for the determination of the unknown integer vector \mathbf{s} , it cannot be ignored that the choice of \mathbf{s} (i.e., the type, the size, and the nature of the array clusters/tiles) significantly impacts on the costs of the resulting arrangements [6], thus it cannot be totally free and the designer must be allowed to specify what *classes* of clusters (e.g., the sizes and/or the shapes as well as contiguous/non-contiguous types) has/have to be used as building block/s for the arising 5G architecture.

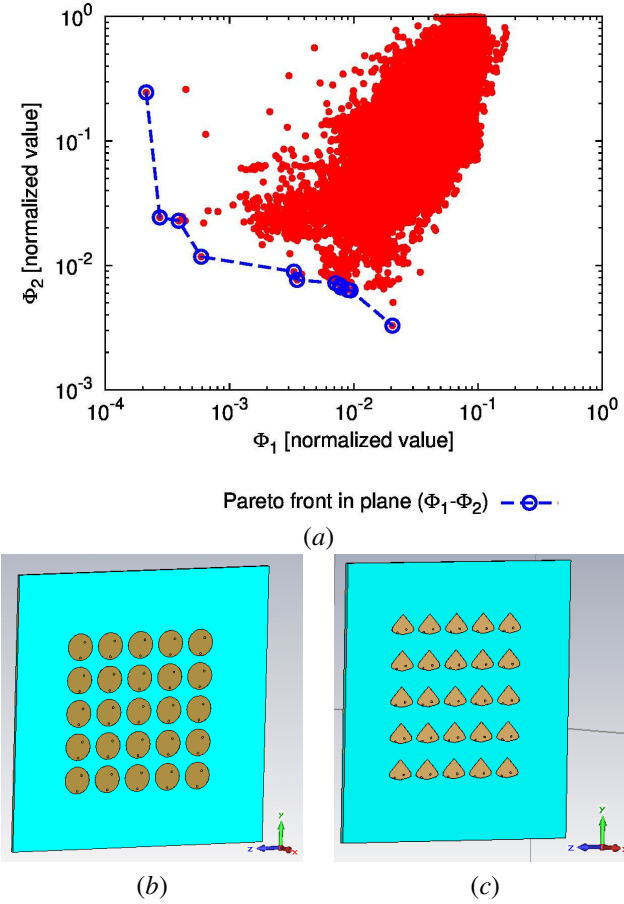


Figure 5. Antenna element synthesis phase (Rectangular lattice, $0.492\lambda_0 \times 0.651\lambda_0$ unit cell) - Plots of the representative points of a set of ε -MOEA solutions in the $(\tilde{\Phi}_1, \tilde{\Phi}_2)$ plane and associated Pareto fronts (a), and geometries of selected Pareto-optimal tradeoff solutions (b)(c) as modeled in *CST Microwave Studio*.

Therefore, the *5G Array Clustering* problem is formulated as that of finding the best combination of Q clusters taken from an *alphabet* of D user-defined sub-arrays [19] such that (7) is minimized. Due to discrete nature of the problem unknowns, s_n , $n = 1, \dots, N$, it would be quite natural to consider as optimization solver [24][30][31] a binary *GA* [25][26] in which the membership of the generic n -th array element, q , is encoded into a string of $\lceil \log_2 D \rceil$ bits [19]. However, this choice would be numerically ineffective since it would result in *GA* individuals with chromosomes of $\lceil \log_2 D \rceil \times Q$ bits (i.e., proportional to the size of the alphabet and the aperture) potentially causing *GA* convergence issues [24] because of their long length when implemented for medium/large arrays as those in 5G applications. In order to prevent these latter, an Integer-Coded *SO-GA* strategy is adopted hereinafter, the shape/size choice of the q -th cluster in the p -th ($p = 1, \dots, P$; P being the *GA* population size) *GA* individual at the i -th iteration ($i = 1, \dots, I$; I being the maximum number of *GA* iterations), $\mathbf{d}^{p,i} \triangleq \{d_q^{p,i}; q = 1, \dots, Q\}$, being encoded in an integer variable, $d_q^{p,i} \in [1, D]$ thus reducing the overall length of the chromosome to Q as well as the dimension of the searching space from $2^{\lceil \log_2 D \rceil \times Q}$ down to D^Q . The price to pay for this choice is the need to customize the standard *GA*

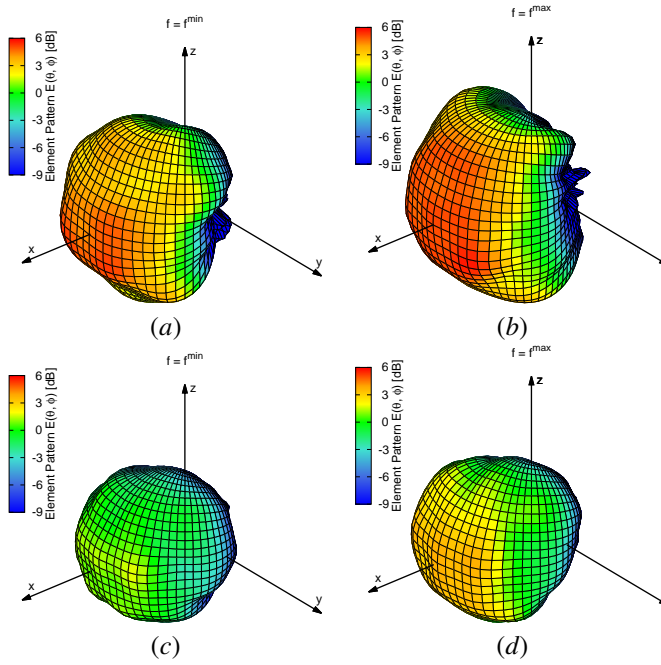


Figure 6. Antenna element synthesis phase (Rectangular lattice, $0.492\lambda_0 \times 0.651\lambda_0$ unit cell) - Behaviour of $E(\theta, \varphi; f)$ for (a)(c) tradeoff solution in Fig. 5(b) and (a)(c) tradeoff solution in Fig. 5(c) when (a)(b) $f = f^{\min}$ and (c)(d) $f = f^{\max}$.

operators to such an Integer-Coded SO-GA. More specifically (Fig. 2),

- *Mutation* - If the p -th individual is selected for mutation (η being the mutation probability), the q -th gene of the corresponding chromosome (i.e., the q -th tile of the p -th clustering solution) is randomly mutated with probability μ by setting $d_q^{p,i}$ to a random integer value in the range $[1, D]$;
- *Decoding (Array Tiling)* - At the i -th iteration, each gene $d_q^{p,i}$ ($q = 1, \dots, Q$) is firstly decoded into the corresponding cluster shape/size/orientation according to a strategy inspired by [19] and considering the alphabet look-up table in Fig. 3. In short, the p -th clustered arrangement corresponding to the p -th GA individual at the i -th iteration, $s^{p,i}$, is generated by placing the Q clusters within the aperture such that the first tile is located in the top-right edge of the aperture, while the following ones are distributed over the array surface through a circular (clockwise) placement by taking into account the location of already clustered elements and exploiting a quadrant symmetry (Fig. 3);
- *Cost Function Evaluation* - The optimal excitations $[\mathbf{a}(s^{p,i}), \Psi(s^{p,i})]^{opt}$ of the clustering scheme $s^{p,i}$ are computed by solving (14) with a standard convex programming tool [29] and the corresponding cost function value $\Phi_{SO}^{p,i}$ is determined by substituting $s^{p,i}$ and $[\mathbf{a}(s^{p,i}), \Psi(s^{p,i})]^{opt}$ in (12), $\Phi_{SO}^{p,i} \triangleq \Phi_{SO}(s^{p,i}, \mathbf{a}(s^{p,i}), \Psi(s^{p,i}))$;
- *Convergence Check* - The GA procedure is iterated until

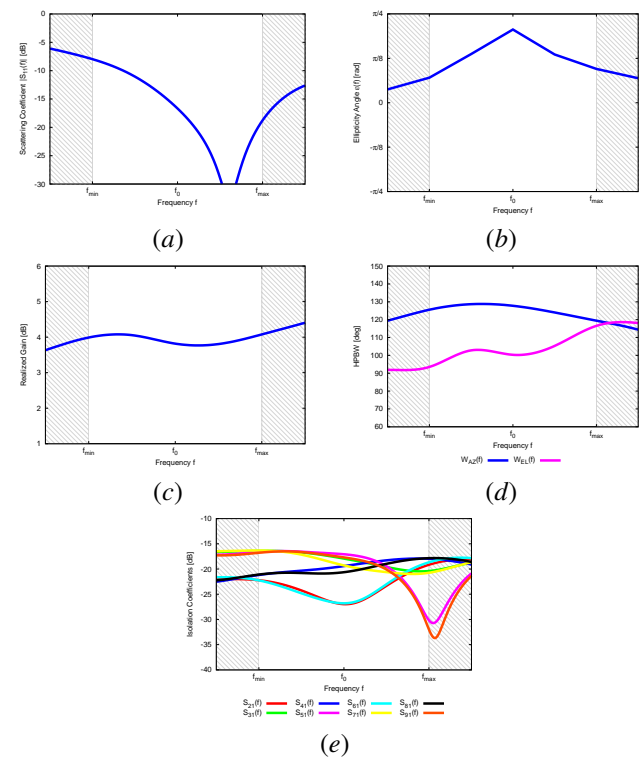


Figure 7. Antenna element synthesis phase (Rectangular lattice, $0.492\lambda_0 \times 0.651\lambda_0$ unit cell) - Behaviour of the full-wave numerical simulated (a) $|S_{11}(f)|$, (b) $\epsilon(f)$, (c) realized gain, (d) $W_{AZ}(f)$ and $W_{EL}(f)$, and (e) $|S_{k1}(f)|$ ($k = 2, \dots, 9$) for the tradeoff configuration in Fig. 5(b).

either $i = I$ or

$$\frac{|\Phi_{SO}^{(I)} - \sum_{i=\mathcal{I}-\widehat{\mathcal{I}}}^{\mathcal{I}} \Phi_{SO}^{(i)}|}{\Phi_{SO}^{(I)}} \leq \tau \quad (15)$$

where $\Phi_{SO}^{(I)} \triangleq \min_{p=1, \dots, P; i=1, \dots, \mathcal{I}} \{\Phi_{SO}^{p,i}\}$ is the cost function value of the “global best” individual at the iteration \mathcal{I} , while $\widehat{\mathcal{I}}$ and τ are the convergence window and the convergence threshold, respectively.

As for the *Selection* and *Crossover* operators, standard roulette-wheel implementations and (integer-coded) single-point crossover with crossover probability χ are adopted [24]. It is worth pointing out that choosing such an optimization strategy (i) enables the user to *a-priori* specify, by defining the tile alphabet, the cluster shapes compliant with the technological constraints of the reference 5G implementation as well as the cost concerns towards the large-scale base station production and (ii) it minimizes the dimension of the search space, thus mitigating the convergence issues of the optimization when large apertures are of interest.

B. “Antenna Element Synthesis“ Step (ε -MOEA)

As for the second step of the *co-design* process, it consists of a *MMO continuous* optimization problem since it involves the joint minimization of $L - 1$ cost function terms [i.e., $\Phi_{MMO}(\mathbf{g})$ - 13] to determine the optimal values of the (continuous) geometrical parameters of the array element.

A key mechanism of this procedural step is the so-called “antenna geometry generator” (AGG), which is responsible to encode/decode the shape of the antenna element starting from the corresponding vector of geometrical parameters \mathbf{g} [16]. The requirements for such an operator are that, on the one hand, a wide set of structures should be modeled to allow the exploration of different geometries during the design phase [Fig. 1(b)] and, on the other hand, a small number of descriptors, M , should be enough for faithfully identifying the radiator shape in order to keep low the dimensionality of the optimization problem thus avoiding complex and time-expensive searches in the sampling the search space looking for the optimal solution. According to these inputs and following the guidelines adopted for the design of stand-alone wideband antenna systems [16], the chosen AGG operator is the result of a combination of “parametric” and “spline”-based descriptors used, the former, to describe the cavity radius, g_1 , and the cavity height, g_2 , as well as the probe feed position in the yz -plane, (g_3, g_4) [Fig. 1(c)] and, the latter, to encode complex antenna contours through spline curves with $\frac{M-4}{2}$ control points in the yz -plane, $(g_m, g_{m+\frac{M-4}{2}})$, $m = 5, \dots, M - \frac{M-4}{2}$ [Fig. 1(b)]. Of course, such a modelling would be enough (at least in principle) when dealing with stand-alone radiators [16], but it is unsatisfactory when addressing synthesis problems such as that for 5G systems and, even more, when the design result is not limited to a lab-controlled experiment, but it must be close to the final manufacturing, thus numerically predicting real world impacts and guaranteeing a reliable working. More in detail, unlike the stand-alone design, the solution of (13) must manage shape/size constraints that vary depending on the solution to the *SO discrete* problem (12) iteratively carried out in the co-design *array clustering* phase (Sect. III-C). Moreover, the evaluation of the *mutual* interactions among nearby radiators when arranged in a finite array layout is mandatory (13), as well. To properly face with those difficulties, it is needed to couple the AGG operator with another one [here called *System Characterization* (SC) operator] able to model the elementary radiator by taking into account spacing constraints coming from the *array clustering* block and to reliably estimate the inter-element isolation/coupling parameters by considering the *finite* size of the final arrangements, that is, without recurring to simplified periodic models for the array structure. Towards this end, an *extended finite* model is introduced [Fig. 4(a)] where the radiator “shape” coming from the AGG operator is surrounded by a set of H “rings” of identical elements (H being selected according to a parametric analysis to guarantee that a good tradeoff between computational complexity and accuracy is achieved - Sect. IV-A) and the coupling/isolation parameters as well as the average pattern $E(\theta, \varphi; f)$ are evaluated by feeding only the central element of such a H -size set. It is worth highlighting that the exploitation of a *finite array* model instead of a stand-alone or periodic configuration guarantees a reliable and faithful synthesis of the radiating element, which does not need further element re-optimization when the same radiator is placed within the whole array arrangement since both the figures of merit and the average

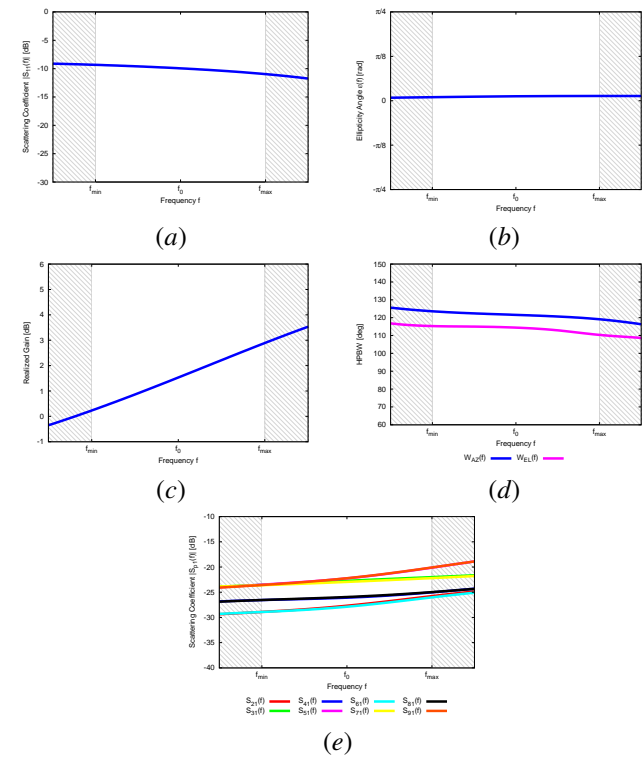


Figure 8. Antenna element synthesis phase (Rectangular lattice, $0.492\lambda_0 \times 0.651\lambda_0$ unit cell) - Behaviour of the full-wave numerical simulated (a) $|\mathcal{S}_{11}(f)|$, (b) $\varepsilon(f)$, (c) realized gain, (d) $W_{AZ}(f)$ and $W_{EL}(f)$, and (e) $|\mathcal{S}_{k1}(f)|$ ($k = 2, \dots, 9$) for the tradeoff configuration in Fig. 5(c).

pattern $E(\theta, \varphi; f)$ so computed are equal or very close to the all-array ones.

Concerning the optimization mechanism (i.e., the other key tool of the co-design phase III-C), it could be straightforwardly solved by a *MMO continuous* solution strategy, but directly solving (13) is a challenging task because of the cost/complexity of the solution space exploration, which is further and significantly increased by the number of objectives when greater than $L = 4$, and the limited availability of fast and efficient *MMO* algorithms [32]. Thus, the original *MMO* is reformulated in the following multi-objective (*MO*) one

$$\Phi_{MO}(\mathbf{g}) \triangleq \left\{ \tilde{\Phi}_l(\bar{\mathbf{s}}, \bar{\mathbf{a}}, \bar{\Psi}, \mathbf{g}), l = 1, 2, 3 \right\} \quad (16)$$

by aggregating, according to their physical “coherence”, the components of $\Phi_{MMO}(\mathbf{g})$ into the the following cost function terms:

- *Impedances* Term

$$\begin{aligned} \tilde{\Phi}_1(\bar{\mathbf{s}}, \bar{\mathbf{a}}, \bar{\Psi}, \mathbf{g}) &\triangleq \xi_2 \Phi_2(\bar{\mathbf{s}}, \bar{\mathbf{a}}, \bar{\Psi}, \mathbf{g}) + \\ &+ \sum_{l=7}^L \xi_l \Phi_l(\bar{\mathbf{s}}, \bar{\mathbf{a}}, \bar{\Psi}, \mathbf{g}); \end{aligned} \quad (17)$$

given by the weighted combination of self- and mutual-impedances terms;

- *Beam Directionality* Term

$$\tilde{\Phi}_2(\bar{\mathbf{s}}, \bar{\mathbf{a}}, \bar{\Psi}, \mathbf{g}) \triangleq \sum_{l=4}^6 \xi_l \Phi_l(\bar{\mathbf{s}}, \bar{\mathbf{a}}, \bar{\Psi}, \mathbf{g}); \quad (18)$$

yielded from the combination of the beamwidth and the realized gain terms;

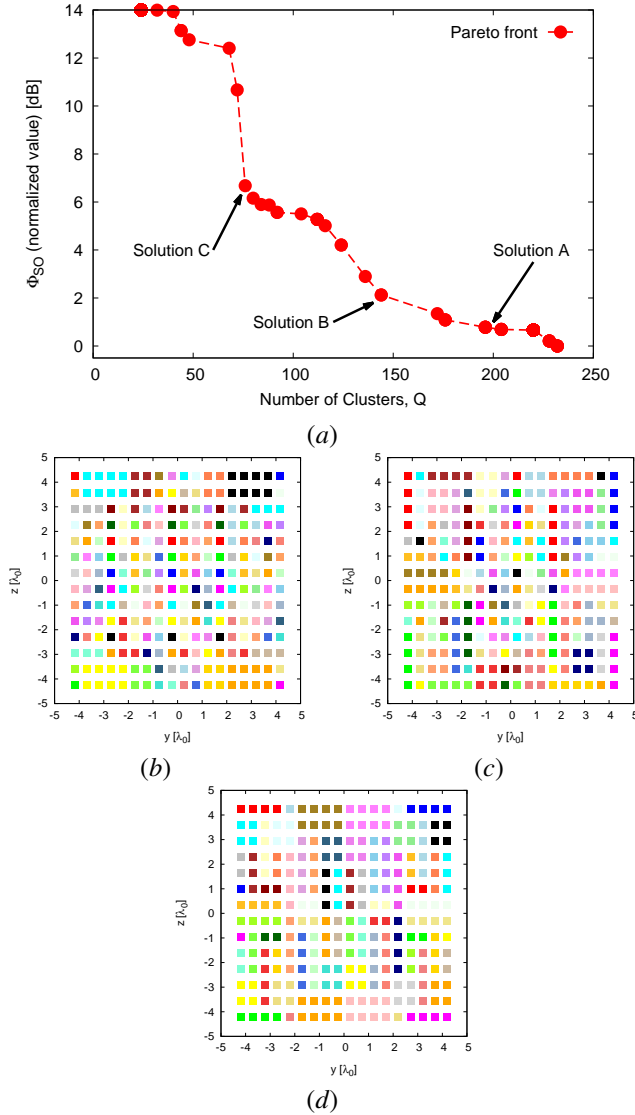


Figure 9. *Array clustering phase* (Rectangular lattice, $0.492\lambda_0 \times 0.651\lambda_0$ unit cell, $N = 18 \times 14$, Fig. 5(b) embedded radiator) - Plots of the representative points of a set of SO-GA solutions in the (Φ_{SO}, Q) -plane and associated Pareto fronts (a), and layouts of selected Pareto-optimal tradeoff clustered arrangements (each color identifying a different cluster) with (b) $Q = 196$, (c) $Q = 144$, and (d) $Q = 76$.

• *Polarization Term* - $\tilde{\Phi}_3(\bar{s}, \bar{a}, \bar{\Psi}, g) \triangleq \xi_3 \Phi_3(\bar{s}, \bar{a}, \bar{\Psi}, g);$
 $\xi_l, l = 2, \dots, L$, being user-defined real weighting coefficients. Being the dimension of the non-linear MO problem reduced to $L = 3$ (16), the version of ε -MOEA optimization tool in [33] is applied since it proved to be effective for a global search in continuous spaces [21][22] and to enable quick convergence, while maintaining a well-distributed set of non-dominated solutions during the iterative optimization process.

C. Co-Design Algorithmic Implementation

The *alternate two-step co-design* approach (Fig. 2) includes the “*Array Clustering*“ (Sect.) and the “*Antenna Element Synthesis*“ (Sect.) steps within the following iterative process:

- *Initialization* - The values of the array lattice and the aperture width are set by exploiting state-of-the-art analytical formulas [7] to avoid grating lobes within the 5G angular steering range and bandwidth as well as to guarantee the required target directivity;
- “*Antenna Element Synthesis*“ - A set of Pareto-optimal trial antenna shapes is determined by minimizing the cost function $\tilde{\Phi}_{MO}(g)$ (16) by means of the ε -MOEA. Towards this end, the multi-objective optimization strategy samples the search space by generating at each iteration W candidate configurations $g^w, w = 1, \dots, W$, which are ranked through the following operations
 - *Radiator Geometry Generation* - The AGG operator infers from g^w (Sect. III-C) the shape of the corresponding array element (Sect. III-C);
 - *Cost function Computation* - The radiator shape deduced from g^w is surrounded with H rings of identical antennas [Fig. 4(a)] and the SC operator (Sect. III-C) is applied to evaluate the corresponding value of (16);
- “*Array Clustering*“ - Starting from the array element synthesized at the convergence of the previous ε -MOEA optimization, the Integer-Coded SO-GA optimization is run by iteratively applying the operators described in Sect. III-C. More specifically, after a random initialization of the initial population, $\{d^{p,0}; p = 1, \dots, P\}$, the *Selection*, the *Crossover*, the *Mutation*, the *Decoding*, and the *Elitism* operators [24] are iteratively applied ($i = 1, \dots, I$) to generate a new set of trial solutions, $\{d^{p,i}; p = 1, \dots, P\}$ (Fig. 2), which are then ranked according to their fitness (12) values, until the *Convergence Check* condition holds true;
- “*Array Improvement*“ - The aperture/inter-element spacing are reduced by a user-defined scaling factor to minimize the array dimensions and the *co-design* loop is repeated starting from the “*Antenna Element Synthesis*“ phase until the array design is compliant with the 5G user-defined specifications or the maximum number of iterations is reached.

IV. NUMERICAL RESULTS

Representative synthesis examples drawn from on-going projects are presented in this section to prove the effectiveness of the proposed *co-design* strategy in designing new *unconventional* array architectures and array elements to be used in real-world 5G base stations (i.e., completely different from traditional solutions in terms of array layout/capabilities and element performance [2]) as well as to assess the reliability of such an approach in taking into account the impact of mutual coupling, non-ideal antenna patterns, and implementation limitations. As for the 5G design requirements, the following setup has been assumed: $S_{11}^T = -10$ [dB], $\varepsilon^T = 0$ [deg] (linear polarization), $W_{AZ}^T = 120$ [deg], $W_{EL}^T = 90$ [deg], $G^T = 4$ [dB], $S_{k1}^T = 20$ [dB], $\{\theta_0^{\min} = 67.5$ [deg], $\theta_0^{\max} = 112.5$ [deg]; $\varphi_0^{\min} = -60$ [deg], $\varphi_0^{\max} = 60$ [deg]\} (cellular sector coverage), $\mathcal{P}^T(\theta, \varphi; \theta_0, \varphi_0) = -15$ [dB] sidelobe level in the

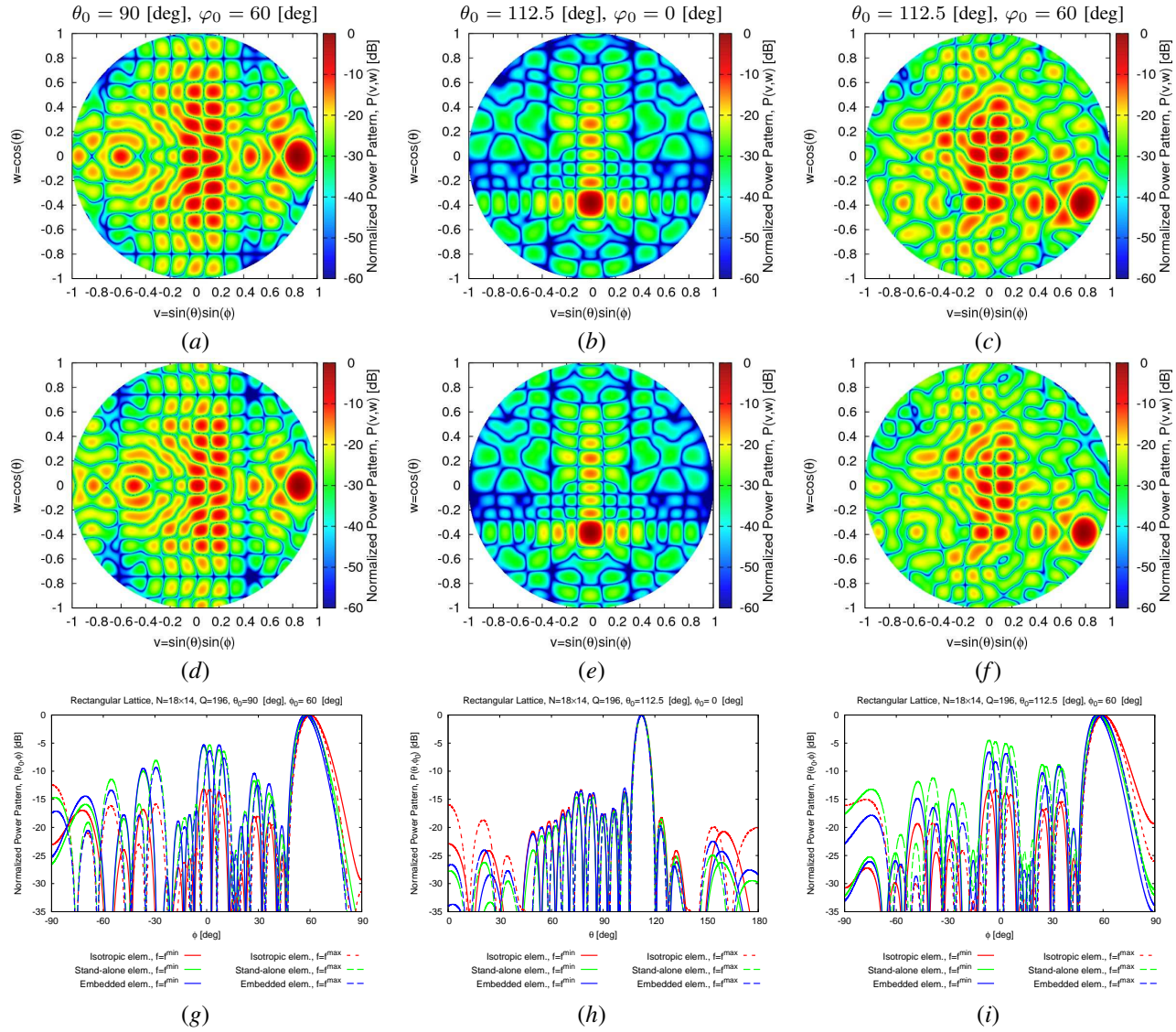


Figure 10. Array clustering phase (Rectangular lattice, $0.492\lambda_0 \times 0.651\lambda_0$ unit cell, $N = 18 \times 14$, $Q = 196$) - Plots of $\mathcal{P}(\theta, \varphi; \theta_0, \varphi_0; f)$ assuming the “embedded” element in Fig. 5(b) at (a)(b)(c) $f = f^{\min}$ and (d)(e)(f) $f = f^{\max}$, (g)(h)(i) associated “cuts” versus φ when (a)(d)(g) $(\theta_0, \varphi_0) = (90, 60)$ [deg], (b)(e)(h) $(\theta_0, \varphi_0) = (112.5, 0)$ [deg], and (c)(f)(i) $(\theta_0, \varphi_0) = (112.5, 60)$ [deg], and (g)(h)(i) comparisons with “isotropic” and “stand-alone” radiators.

entire visible range, and⁵ $f^{\max} = 1.1f^{\min}$.

A. Calibration of the Extended Finite Array Model

This sub-section reports some results of the numerical calibration of the *extended finite array* model. Such a study is aimed at determining the number of rings H surrounding the reference radiator that guarantees a suitable tradeoff between (a) complexity of the resulting model to be simulated with a full-wave numerical solver in the *SC* operator and (b) numerical-stability and accuracy of the corresponding isolation parameters $\mathcal{S}_{k1}(f)$, $k = 2, \dots, 9$, quantifying the electromagnetic coupling and impact among a single array element and its

⁵Hereinafter, all geometrical parameters are/will be expressed in terms of the central frequency wavelength, $\lambda_0 = \frac{c}{f_0}$, being $f_0 \triangleq \frac{f^{\max} + f^{\min}}{2}$. Because of a NDA, the value of f_0 cannot be made explicit, but it is worth pointing out that this does not limit the contribution of this work since all considerations and outcomes can be fruitfully applied to any potential 5G band.

surroundings [Fig. 4(a)]. Towards this end, a set of identical standard circular patch antennas [34] displaced in a regular lattice with rectangular unit cells sided $0.492\lambda_0 \times 0.651\lambda_0$ [7] to avoid the presence of grating lobes in the visible range when $f \in [f^{\min}, f^{\max}]$, $\theta_0 \in [\theta_0^{\min}, \theta_0^{\max}]$, $\varphi_0 \in [\varphi_0^{\min}, \varphi_0^{\max}]$) has been simulated with a full-wave solver. The values of the isolation parameters, $\mathcal{S}_{k1}(f)$, $k = 2, \dots, 9$, have been numerically computed through *CST* solvers [Figs. 4(b)-4(c)] and their values compared when varying H [Fig. 4(a)].

The plots of the $\mathcal{S}_{21}(f)$ parameter in the frequency band $f \in [f^{\min}, f^{\max}]$ and for various values of H [Fig. 4(b)] indicate that non-negligible variations arise until $H < 3$, while a more stable behaviour holds true from $H = 3$ (i.e., a neighbourhood of more than 5×5 elements). Further increasing the neighbourhood size ($H \geq 4$) does not significantly affect the simulation outcomes [i.e., $|\mathcal{S}_{21}(f)|_{H=3} - \mathcal{S}_{21}(f)|_{H=4}| \leq 0.5$ [dB] when $f \in [f^{\min}, f^{\max}]$ - Fig. 4(b)]. Similar conclusions can be drawn also from the behaviours of the other coefficients,

$\mathcal{S}_{k1}(f)$, $k > 2$, as shown in Fig. 4(b) for $\mathcal{S}_{51}(f)$. Thus, the threshold value $H = 3$ is adopted as a suitable tradeoff between accuracy and computational efficiency since enlarging the neighbouring set H does not significantly modify the computed values of $\mathcal{S}_{k1}(f)$, $k = 2, \dots, 9$, while it increases the computational burden.

B. Element Synthesis and Array Clustering

The first benchmark design is concerned with a 5G radiating system of $N = 18 \times 14$ elements distributed over a lattice characterized by a $0.492\lambda_0 \times 0.651\lambda_0$ rectangular unit cell. Moreover, the *Rogers 3035* has been chosen as substrate material and a standard Teflon-filled coaxial cable has been used for feeding each elementary radiator.

At the convergence of the alternate two-step co-design (Sect. III-C), the outcome from the “Antenna Element” block is the plot of the representative points in the $(\tilde{\Phi}_1, \tilde{\Phi}_2)$ -plane [Fig. 5(a)] yielded through the ε -MOEA by setting $\xi_l = 1.0$, $l = 2, \dots, L$ along with the associated Pareto (blue line). Although $\tilde{\Phi}_1 > 10^{-4}$ and $\tilde{\Phi}_2 > 10^{-3}$ [Fig. 5(a)], there are several candidate elementary antennas showing excellent tradeoff performance. To better appreciate the effectiveness of the array element synthesis, let us analyze two tradeoff solutions [Figs. 5(b)-5(c)] of the Pareto front. With reference to an $H = 3$ finite-array model and a *CST* full-wave simulation of the devices, Figure 6 gives the radiated element factors, $E(\theta, \varphi; f)$, which, as expected, present a broad and stable main beam within the whole band of interest [e.g., $f = f^{\min}$ - Fig. 6(a) and Fig. 6(c); $f = f^{\max}$ - Fig. 6(b) and Fig. 6(d)]. Such a feature, which is of fundamental importance in AESA-based 5G base station for having a full angular coverage in azimuth and elevation, is also quantitatively confirmed by the values of the associated half-power beamwidths: $W_{AZ}^T(f) > W_{EL}^T(f) > W_{EL}^T$ [Fig. 7(d) and Fig. 8(d)]. It is worth noticing that this is a necessary condition for allowing the array to steer along the desired direction (θ_0, φ_0) and, being such a result obtained when considering the *extended finite-array* model, it holds true also when the radiator is inserted in the actual array geometry, thus without the need of a further re-optimization because of the presence of other array elements.

As for the element impedance, the plot in Fig. 7(a) shows that the tradeoff configuration in Fig. 5(b) is able to yield $\mathcal{S}_{11}(f) \leq \mathcal{S}_{11}^T$ almost in the whole band $f \in [f^{\min}, f^{\max}]$ and that a deep resonance appears around $f = 1.07f^{\min}$. Otherwise, the radiator in Fig. 5(c) guarantees a more stable impedance trend without strong resonances within the working frequency band [Fig. 8(a)], but with a value quite close to \mathcal{S}_{11}^T .

On the other hand, when comparing the plots of the polarization ellipticity [Fig. 7(b) vs. Fig. 8(b)], it turns out that the design in Fig. 5(c) results in a very effective polarization control [i.e., $\varepsilon(f) \approx \varepsilon^T = 0$ [deg] - Fig. 8(b)], while the one in Fig. 5(b) quite significantly deviates from ε^T [Fig. 7(b)].

Concerning the realized gain [Fig. 7(c) vs. Fig. 8(c)], the solution in Fig. 5(b) reasonably fits the project requirement G^T [Fig. 7(c)], while this latter is satisfied only around $f = f^{\max}$

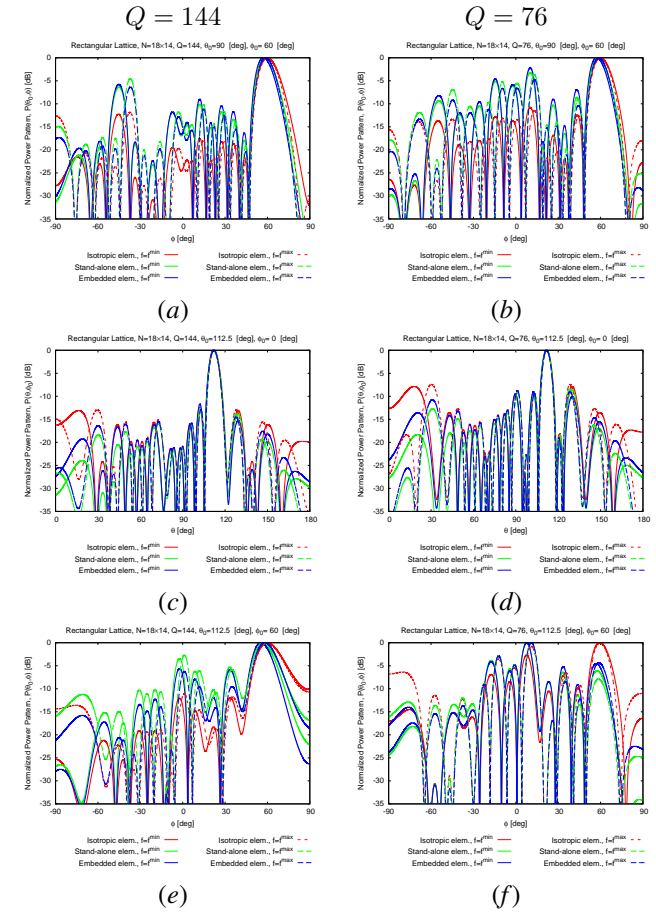


Figure 11. Array clustering phase (Rectangular lattice, $0.492\lambda_0 \times 0.651\lambda_0$ unit cell, $N = 18 \times 14$) - Pattern cuts of $\mathcal{P}(\theta, \varphi; \theta_0, \varphi_0; f)$ assuming the “embedded” element in Fig. 5(b) and comparisons with “isotropic” and “stand-alone” radiators when (a)(b) $(\theta_0, \varphi_0) = (90, 60)$ [deg], (c)(d) $(\theta_0, \varphi_0) = (112.5, 0)$ [deg], and (e)(f) $(\theta_0, \varphi_0) = (112.5, 60)$ [deg] for (a)(c)(e) $Q = 144$, and (b)(d)(f) $Q = 76$.

[Fig. 8(c)] for the geometry in Fig. 5(c) as also visible in the corresponding element patterns [Fig. 6].

Since the project requirements have been ranked from the impedance matching down to the polarization passing through the isolation coefficients, the HPBW, and the realized gain, the geometry in Fig. 5(b) is the “selected” tradeoff configuration for the final design. Nevertheless, it is worthwhile to remark that any of the obtained tradeoff geometries in Fig. 5(a) can be chosen by the user since all of them are “non-dominated” in the Pareto sense.

Dealing with the clustering of the $N = 18 \times 14$ arrangement of the synthesized array elements [Fig. 5(b)], an *alphabet* of potential sub-arrays comprising only square/rectangular cluster geometries with dimensions from 1×1 up to 7×7 ($D = 49$) has been defined. Such an alphabet has been chosen to take into account some limitations arising in the implementation of 5G systems and concerned with the arrangement modularity and the cost reduction with respect to the fabrication of all different and customized tiles.

Before analyzing the results of the SO-GA optimization, let us first notice that the choice of such an integer-coded version allows one a significant computational saving of the order

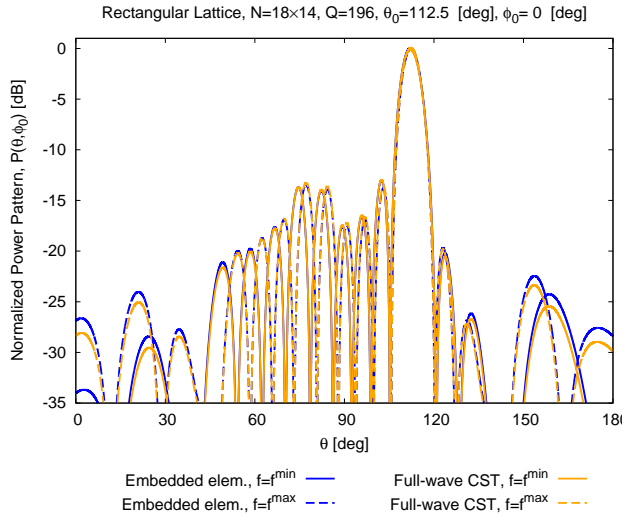


Figure 12. Array clustering phase (Rectangular lattice, $0.492\lambda_0 \times 0.651\lambda_0$ unit cell, $N = 18 \times 14$, $Q = 196$, $(\theta_0, \varphi_0) = (112.5, 0)$ [deg]) - Plots simulated $\mathcal{P}(\theta, \varphi; \theta_0, \varphi_0; f)$ and comparisons with CST full-wave modeling.

of 5.5×10^{22} in magnitude with respect to a binary-coded implementation of the same approach. Let us now analyze the plot of the Pareto front of the SO-GA solutions in the (Φ_{SO}, Q) -plane [Fig. 9(a)] generated by varying the GA control parameters (i.e., P , χ , η , μ , \mathcal{I} , $\widehat{\mathcal{I}}$, and τ) and enforcing a target sidelobe equal to -14 [dB]. As it can be observed, increasing the number of sub-arrays Q gives a reduction of the array pattern mismatch, as physically expected. Moreover, an excellent pattern control in the whole frequency and angular ranges (i.e., $\Phi_{SO} \approx 0$) can be yielded with $Q \approx 220$ clusters (i.e., a clustering factor $\nu \triangleq \frac{Q}{N} \approx 85\%$ corresponding to a 15% reduction of the control points with respect to the fully-populated counterpart) despite the very wide field-of-view. Furthermore, many different tradeoff solutions can be deduced [Fig. 9(a)] which allow the 5G system designer to select the most proper configuration in terms of architectural complexity and achievable performance.

For illustrative purposes, the geometrical/electrical/radiation features of three representative arrangements, denoted as Solution “A”, Solution “B”, and Solution “C” in Fig. 9(a), are reported in the following. The first comment on the physical arrangements corresponding to the “Solution A” [$Q = 196$ - Fig. 9(b)], the “Solution B” [$Q = 144$ - Fig. 9(c)], and the “Solution C” [$Q = 76$ - Fig. 9(d)] is that all are non-regularly clustered schemes even though generated starting from modular sub-arrays. Such a feature plays a key role in mitigating/avoiding quantization lobes [6][7], which can potentially appear as a consequence of a clustered architecture [Fig. 1(a)]. For instance, the array pattern radiated at $f = f^{min}$ by the $Q = 196$ clustered arrangement [Fig. 9(b)] when $(\theta_0, \varphi_0) = (90, 60)$ [deg] [Fig. 10(a)] shows that, despite the steering at the edge of the field-of-view along the azimuth plane and the unavoidable scan losses also caused by the non-ideal nature of the radiating element, all the secondary lobes are below the mainbeam [Fig. 10(a)]. Such a result is also confirmed when $f = f^{max}$ [Fig. 10(d)]. Similar or better

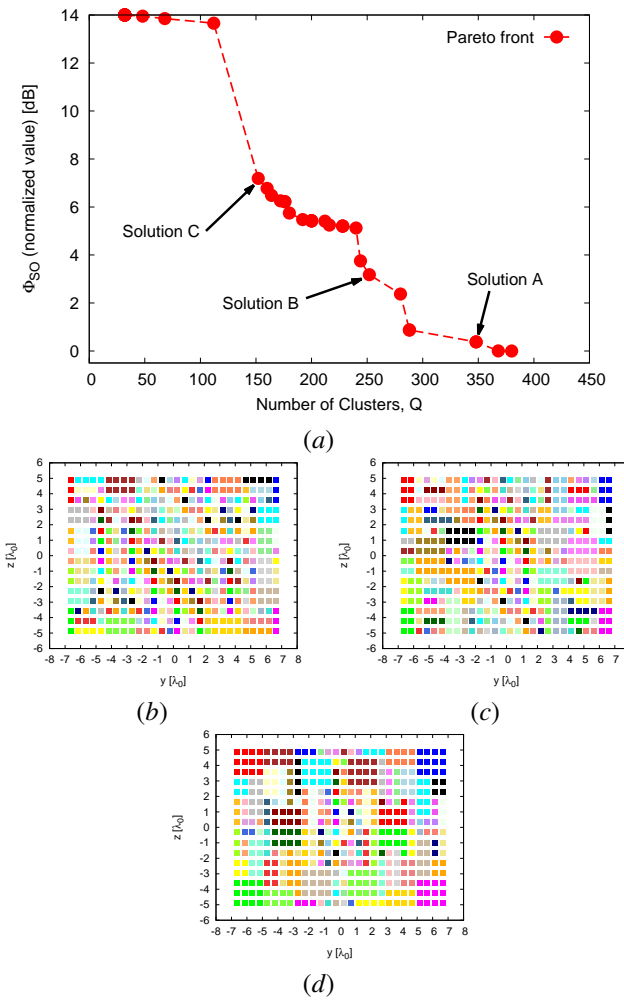


Figure 13. Array clustering phase (Rectangular lattice, $0.492\lambda_0 \times 0.651\lambda_0$ unit cell, $N = 28 \times 16$, Fig. 5(b) embedded radiator) - Plots of the representative points of a set of SO-GA solutions in the (Φ_{SO}, Q) -plane and associated Pareto fronts (a), and layouts of selected Pareto-optimal tradeoff clustered arrangements (each color identifying a different cluster) with (b) $Q = 348$, (c) $Q = 252$, and (d) $Q = 152$.

outcomes [Fig. 10(h) vs. Fig. 10(g)] hold true when steering along the elevation plane [i.e., $(\theta_0, \varphi_0) = (112.5, 0)$ [deg] - $f = f^{min}$, Fig. 10(b); $f = f^{max}$, Fig. 10(e)], as well, since the field-of-view in θ is significantly narrower than in φ ($\theta_0^{max} - \theta_0^{min} = 45$ [deg] vs. $\varphi_0^{max} - \varphi_0^{min} = 120$ [deg]). It is also worthwhile to remark that the SO-GA “Solution A” guarantees an acceptable sidelobe control also in the most challenging scenario (i.e., when $f = f^{max}$, $\theta_0 = \theta_0^{max}$, $\varphi_0 = \varphi_0^{max}$ - Fig. 10(f)]. Indeed, no grating lobe/quantization lobes above the mainlobe appear at any frequency [Fig. 10(c) and Fig. 10(f)]. These considerations confirm that the proposed co-design strategy enables the synthesis of 5G base station arrangements with significantly simplified architectures (e.g., $\nu \approx 77\%$) without significant performance loss in terms of mainbeam and sidelobe control despite the very wide field-of-view at hand.

A further reduction of the architecture complexity (i.e., smaller Q values) can be reached by selecting different trade-off configurations of the SO-GA Pareto front [Fig. 9(a)] as for

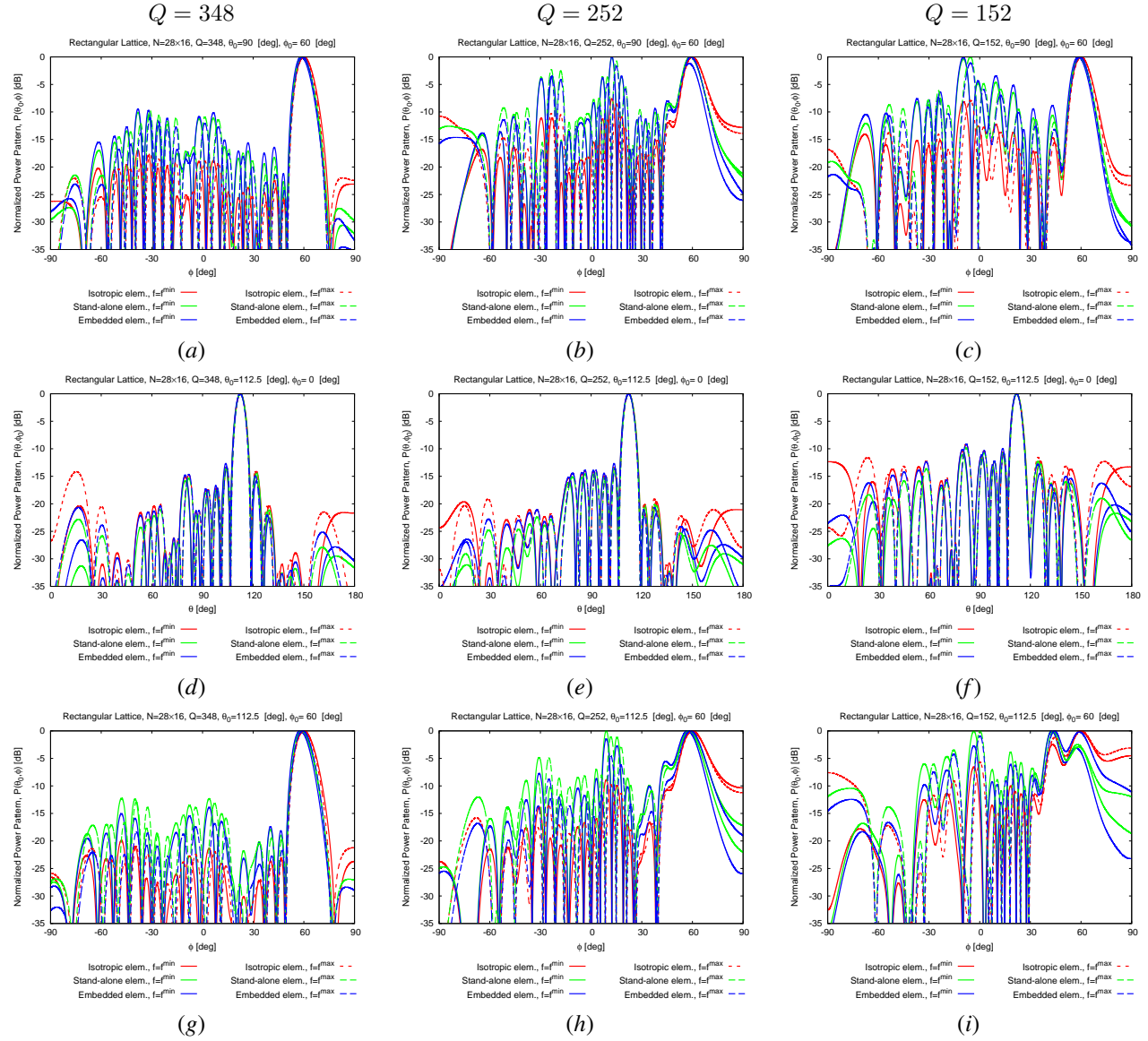


Figure 14. Array clustering phase (Rectangular lattice, $0.492\lambda_0 \times 0.651\lambda_0$ unit cell, $N = 28 \times 16$) - Plots $\mathcal{P}(\theta, \varphi; \theta_0, \varphi_0; f)$ assuming the “embedded” element in Fig. 5(b) and comparisons with “isotropic” and “stand-alone” radiators when (a)(b)(c) $(\theta_0, \varphi_0) = (90, 60)$ [deg], (d)(e)(f) $(\theta_0, \varphi_0) = (112.5, 0)$ [deg], and (g)(h)(i) $(\theta_0, \varphi_0) = (112.5, 60)$ [deg] for (a)(d)(g) $Q = 348$, (b)(e)(h) $Q = 252$, and (c)(f)(i) $Q = 152$.

example the “Solution B” (with $Q = 144$) or the “Solution C” (with $Q = 76$) corresponding to a clustering factor equal to $\nu \approx 57\%$ and $\nu \approx 30\%$, respectively. Figure 11 shows that an additional simplification of the array layout causes a loss in the beam control capability, mainly when large values of the steering angle along the azimuth plane are at hand [e.g., $(\theta_0, \varphi_0) = (90, 60)$ [deg] - Fig. 10(g) vs. Fig. 11(a) and Fig. 11(b)]. This causes the possible occurrence of quantization lobes, with magnitude close the main beam in the visible range, and severe pattern degradations as shown Fig. 11(f) for the case with $\nu \approx 30\%$ along the direction $(\theta_0, \varphi_0) = (112.5, 60)$ [deg].

Of course, it cannot be neglected that previous positive results in view of the 5G base station realization are actually enabled by the proposed *co-design* procedure that combines unconventional array design and element synthesis in a single synthesis

loop (Fig. 2). To point out such a key-item, let us compare the radiation patterns from an ideal-elements (i.e., “isotropic” radiators) array or neglecting mutual coupling effects among array elements (i.e., the so-called “stand-alone” configuration). As it can be observed, there are considerable deviations from the *co-design* optimized ones [see “Solution A” - Fig. 10(h); “Solution B” and “Solution C” - Fig. 11], which turn out to be very close to the actual situation as proved in Fig. 12 where, as a representative example, the “Solution A” is compared with the full-wave simulation when $(\theta_0, \varphi_0) = (112.5, 0)$ [deg]. As for this latter comparison, we can reveal a very good agreement at both endpoints of the working frequency range. More in detail, only minor deviations can be observed [≤ 1.5 [dB] - Fig. 12] close to end-fire [i.e., $\theta \rightarrow 0$ [deg] and $\theta \rightarrow 180$ [deg] - Fig. 12] as expected from the theoretical viewpoint since the CST simulation takes into account border effects, as

Table I

Array clustering phase (RECTANGULAR LATTICE, $0.492\lambda_0 \times 0.651\lambda_0$ UNIT CELL, $N = 18 \times 14$) - EFFICIENCY AND GAIN PERFORMANCE ASSUMING “isotropic”, “stand-alone”, AND “embedded” RADIATORS IN FIG. 5(b) AND COMPARISONS WITH CST FULL-WAVE MODELING.

Configuration			Efficiency κ [%]				Gain G [dB]			
Q	f	(θ_0, φ_0) [deg]	Ideal	Stand-Alone	Embedded	CST	Ideal	Stand-Alone	Embedded	CST
196	f^{\min}	(90, 60)	100	98.3	97.9	96.9	24.6	22.1	21.9	22.3
	f^{\max}	(90, 60)	100	97.4	97.0	98.5	24.7	23.1	22.9	23.4
	f^{\min}	(112.5, 0)	100	98.3	97.9	98.3	28.2	28.6	28.4	28.7
	f^{\max}	(112.5, 0)	100	97.4	97.0	95.4	28.5	30.0	28.8	29.0
144	f^{\min}	(90, 60)	100	98.3	97.9	96.7	24.2	21.4	21.2	21.6
	f^{\max}	(90, 60)	100	97.4	97.0	97.1	24.5	22.4	22.2	22.7
	f^{\min}	(112.5, 0)	100	98.3	97.9	98.3	25.1	26.5	26.2	26.7
	f^{\max}	(112.5, 0)	100	97.4	97.0	95.6	25.3	26.6	26.4	26.5
76	f^{\min}	(90, 60)	100	98.3	97.9	97.0	21.8	18.5	19.3	19.9
	f^{\max}	(90, 60)	100	97.4	97.0	98.5	21.7	18.3	19.2	19.8
	f^{\min}	(112.5, 0)	100	98.3	97.9	98.2	22.6	24.2	24.0	24.5
	f^{\max}	(112.5, 0)	100	97.4	97.0	97.5	22.5	24.0	23.9	23.6

well.

The previous considerations are confirmed by the analysis of the array efficiency κ and gain G of the clustered layouts in Fig. 9(b)-9(d) for different frequencies and steering angles (Tab. I). Indeed, (i) for a fixed f and (θ_0, φ_0) , a reduction of Q corresponds to a degradation of the gain (e.g., $G|_{Q=196}^{\text{embed.}} = 21.9$ [dB] vs. $G|_{Q=144}^{\text{embed.}} = 21.2$ [dB] when $(\theta_0, \varphi_0) = (90, 60)$ [deg] and $f = f^{\min}$ - Tab. I), as expected; (ii) the decrease of G is more evident when secondary lobes appear in the visible range [e.g., $G|_{Q=196}^{\text{embed.}} - G|_{Q=144}^{\text{embed.}} \approx 0.7$ [dB] vs. $G|_{Q=144}^{\text{embed.}} - G|_{Q=76}^{\text{embed.}} \approx 4.1$ [dB] when $(\theta_0, \varphi_0) = (90, 60)$ [deg] and $f = f^{\max}$ - see Fig. 11(a) vs. Fig. 11(b) and Tab. I]; (iii) the efficiency of the overall layouts is not significantly affected by Q (e.g., $\kappa|_{Q=144}^{\text{CST}} - \kappa|_{Q=76}^{\text{CST}} \approx 0.3\%$ when $(\theta_0, \varphi_0) = (112.5, 0)$ [deg] and $f = f^{\min}$ - Tab. I); (iv) the “embedded” element model adopted in the co-design process provides a good agreement with full-wave CST computations also in terms of array gain and efficiency (e.g., $|G|_{\text{embed.}}^{\text{CST}} - G|_{\text{CST}}^{\text{CST}}| \leq 0.6$ [dB], $|\kappa|_{\text{embed.}}^{\text{CST}} - \kappa|_{\text{CST}}^{\text{CST}}| \leq 1.5\%$ - Tab. I).

The second design related to another 5G radiating system deals with the same rectangular lattice, but it is concerned with a wider aperture ($N = 28 \times 16$ elements). Since the same unit cell of the first synthesis project is considered, the same element geometry in Fig. 5(b) has been selected as optimal outcome from the *Antenna Element Synthesis* phase. As for the *Array Clustering* phase, the *SO-GA* Pareto front in Fig. 13(a) allows one to draw, besides those discussed in the previous case, the important outcome that, despite the increased problem complexity of the problem at hand due to the wider aperture [$N = 28 \times 16$ - Fig. 13(a) vs. $N = 18 \times 14$ - Fig. 9(a)], very close clustering factors can be yielded with the same pattern mismatch value [e.g., $\Phi_{SO}|_{N=252} = \Phi_{SO}|_{N=448} = 2$ [dB] when $\nu \approx 0.6$ - Fig. 9(a) vs. Fig. 13(a)]. On the other hand, the reduction of the dimension of the search space (i.e., a computational saving in the optimization process) due to the exploitation of the integer-coded *GA* is even wider in this case because of the larger aperture at hand (2.3×10^{40} [$N = 448$, $Q = 348$] vs. 5.5×10^{22} [$N = 252$, $Q = 196$]).

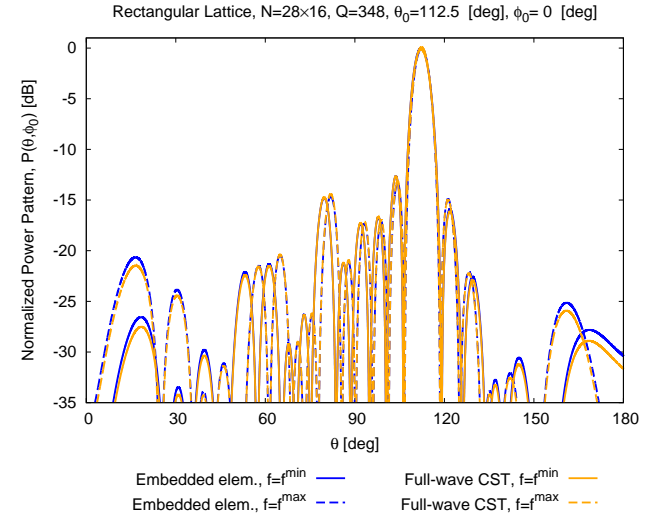


Figure 15. Array clustering phase (Rectangular lattice, $0.492\lambda_0 \times 0.651\lambda_0$ unit cell, $N = 28 \times 16$, $Q = 348$, $(\theta_0, \varphi_0) = (112.5, 0)$ [deg]) - Plots simulated $\mathcal{P}(\theta, \varphi; \theta_0, \varphi_0; f)$ and comparisons with CST full-wave modeling.

For the sake of completeness, the 5G unconventional architectures and the radiation patterns of three representative tradeoff solutions [Solutions “A”, “B”, and “C” - Fig. 13(a)] of the Pareto front in Fig. 13(a) are reported in Figs. 13(b)-13(d) and Fig. 14, respectively. As expected and further confirming the results of the first benchmark on the effectiveness of the proposed co-design scheme, the exploitation of a *SO-GA* irregular clustering scheme with $\nu \approx 77\%$ [$Q = 348$ - Fig. 13(a)] enables an excellent pattern control in all frequencies and steering angles [e.g., $(\theta_0, \varphi_0) = (90, 60)$ [deg] - Fig. 14(a); $(\theta_0, \varphi_0) = (112.5, 0)$ [deg] - Fig. 14(d); $(\theta_0, \varphi_0) = (112.5, 60)$ [deg] - Fig. 14(g)] also thanks to the use of the “finite-array” to model the actual “embedded” element factor, while adopting simplified *isotropic* or *stand-alone* antenna models would yield considerable sidelobe deviations. For example, see Figure 14(d) also taking into account the almost perfect match between the full-wave modelling and the co-designed one in Fig. 15. Further reductions of the architecture complexity [$\nu \approx 56\%$ - Fig. 13(c); $\nu \approx 33\%$ - Fig. 13(d)]

Table II

Array clustering phase (RECTANGULAR LATTICE, $0.492\lambda_0 \times 0.651\lambda_0$ UNIT CELL, $N = 28 \times 16$) - EFFICIENCY AND GAIN PERFORMANCE ASSUMING “isotropic”, “stand-alone”, AND “embedded” RADIATORS IN FIG. 5(b) AND COMPARISONS WITH CST FULL-WAVE MODELING.

Configuration			Efficiency κ [%]				Gain G [dB]			
Q	f	(θ_0, φ_0) [deg]	Ideal	Stand-Alone	Embedded	CST	Ideal	Stand-Alone	Embedded	CST
348	f^{\min}	(90, 60)	100	98.3	97.9	96.5	27.1	24.3	24.1	24.4
	f^{\max}	(90, 60)	100	97.4	97.0	98.2	27.5	25.6	25.5	25.9
	f^{\min}	(112.5, 0)	100	98.3	97.9	98.0	30.7	31.0	30.8	31.2
	f^{\max}	(112.5, 0)	100	97.4	97.0	98.4	31.0	31.4	31.2	31.4
252	f^{\min}	(90, 60)	100	98.3	97.9	97.2	24.4	20.7	20.5	23.1
	f^{\max}	(90, 60)	100	97.4	97.0	98.0	24.5	21.1	21.0	21.8
	f^{\min}	(112.5, 0)	100	98.3	97.9	98.5	29.1	29.7	29.5	29.9
	f^{\max}	(112.5, 0)	100	97.4	97.0	98.3	29.2	29.9	29.7	29.9
152	f^{\min}	(90, 60)	100	98.3	97.9	97.3	22.7	20.4	20.2	20.9
	f^{\max}	(90, 60)	100	97.4	97.0	97.9	23.2	19.2	20.6	21.1
	f^{\min}	(112.5, 0)	100	98.3	97.9	97.5	25.0	25.9	25.7	26.2
	f^{\max}	(112.5, 0)	100	97.4	97.0	97.6	24.7	25.6	25.5	25.4

once again induce non-negligible quantization lobes in the radiation patterns [$Q = 252$ - Fig. 14(b)], mainly at the highest frequencies and far-from-broadside steering angles [e.g., $(\theta_0, \varphi_0) = (112.5, 60)$ [deg], $Q = 152$ - Fig. 14(i)]. Moreover, the values of κ and G of the clustered layouts in Fig. 13(b)-13(d) support the previous conclusions regarding the relation between the array gain and Q (e.g., $G|_{Q=348}^{\text{embed.}} = 24.10$ [dB] vs. $G|_{Q=152}^{\text{embed.}} = 20.21$ [dB] when $(\theta_0, \varphi_0) = (90, 60)$ [deg] and $f = f^{\min}$ - Tab. II) and the reliability of the adopted “embedded” element model (e.g., $|G|_{\text{embed.}}^{\text{embed.}} - G|_{\text{CST}}^{\text{CST}}| \leq 0.8$ [dB] and $|\kappa|_{\text{embed.}}^{\text{embed.}} - \kappa|_{\text{CST}}^{\text{CST}}| \leq 1.4\%$ - Tab. II).

V. CONCLUSIONS AND FINAL REMARKS

Because of the need of suitable tools for the synthesis of unconventional radiating systems for future 5G base stations, a new *co-design* process has been presented where the design of both the antenna element, properly modeled as embedded in a *finite array model*, and the overall array layout are addressed simultaneously. Towards this end, an integer-coded *SO-GA* method for handling irregular array clustering problems with modularity constraints and a customized *MO* antenna-shape-optimization method exploiting an ε -*MOEA* approach have been combined in an alternate iterative loop. A set of representative synthesis examples drawn from on-going projects have been discussed to highlight the features and potentialities of the proposed *co-design* scheme in the solution of 5G array design problems.

The main methodological advancements of this research work with respect to the state-of-the-art include: (i) the development of a new *co-design* framework suitable for simultaneously handling the synthesis of the elementary array antenna and the associated unconventional array architecture; (ii) the derivation of an innovative sub-arrying method based on an integer-coded *GA* able to efficiently explore the solution space, while handling *a-priori* constraints on the admissible cluster geometries/shapes; (iii) the introduction of a *MO* formulation of the 5G single-antenna design that exploits an ε -*MOEA* optimizer and a full-wave (*CST*-based) “finite-array-model” during the whole synthesis process and without recurring to “stand alone” or “periodic” approximated models; (iv) the deduction of

array designs for 5G applications featuring *unconventional* arrangements (i.e., *irregularly/aperiodically* clustered but exploiting modular sub-arrays) to mitigate quantization lobes while significantly reducing the feed network complexity and costs [6] as well as *unconventional* radiators (i.e., combining *spline-contoured* patch antennas and cavity backing) able to simultaneously meet the multiple and contrasting 5G guidelines when embedded in a finite array (unlike conventional state-of-the-art geometries).

With reference to the benchmark designs presented in Sect. IV and concerned with 5G radiating systems, it has been possible to derive the following 5G-array design recipes/guidelines:

- the co-design synthesis of 5G radiating systems can be reliably and effectively carried out by exploiting *finite-array-models* and relatively small simulation domains (i.e., $H = 3$);
- the derivation of an antenna geometry that simultaneously fits all the contrasting requirements arising in 5G scenarios is a very challenging task without a unique solution. Thanks to the co-design synthesis scheme, several tradeoff Pareto-optimal configurations can be found. Therefore, the designer is allowed to choose its “optimal” one, without further re-optimization processes for taking into account mutual coupling effects or array elements interactions, according to his own guidelines, feeling, and requirements;
- analogously to the synthesis of the elementary radiator, the proposed clustering method generates several different *performance-vs-simplicity* tradeoff configurations, once again, at disposal to the array designer. Moreover, the integer coding allows a significant reduction of the dimension of the solution space (5.5×10^{22} - benchmark 1; 2.3×10^{40} - benchmark 2);
- thanks to the proposed unconventional design strategy based on an integer-coded *SO-GA* technique, clustered 5G configurations with significant reduction of the number of control points [e.g., $\nu \approx 77\%$ - Fig. 9(a)] and effective beam control (Fig. 10) are available despite the constraint on the building block sub-arrays. Further architectural simplifications are of course possible whether wider quantization lobes may be tolerated.

Future works, beyond the scope of the current paper, will be aimed at extending the proposed design strategy to fully conformal structures of potential interest for 5G scenarios.

REFERENCES

- [1] M. Jaber, M. A. Imran, R. Tafazolli and A. Tukmanov, "5G backhaul challenges and emerging research directions: A survey," *IEEE Access*, vol. 4, pp. 1743-1766, Apr. 2016.
- [2] C. X. Wang, F. Haider, X. Gao, X.-H. You, Y. Yang, D. Yuan, H. M. Aggoune, H. Haas, S. Fletcher, E. Hepsaydir, "Cellular architecture and key technologies for 5G wireless communication networks," *IEEE Commun. Mag.*, vol. 52, no. 2, pp. 122-130, Feb. 2014.
- [3] D. Muirhead, M. A. Imran, and K. Arshad, "A survey of the challenges, opportunities and use of multiple antennas in current and future 5G small cell base stations," *IEEE Access*, vol. 4, pp. 2952-2964, Apr. 2016.
- [4] F. Boccardi, R. W. Heath, A. Lozano, T. L. Marzetta, and P. Popovski, "Five disruptive technology directions for 5G," *IEEE Commun. Mag.*, vol. 52, no. 2, pp. 74-80, Feb. 2014.
- [5] S. Han, C. I. I., Z. Xu, and C. Rowell, "Large-scale antenna systems with hybrid analog and digital beamforming for millimeter wave 5G," *IEEE Commun. Mag.*, vol. 53, no. 1, pp. 186-194, Jan. 2015.
- [6] P. Rocca, G. Oliveri, R. J. Mailloux, and A. Massa, "Unconventional phased array architectures and design methodologies - A review," *Proc. IEEE*, vol. 104, no. 3, pp. 544-560, Mar. 2016.
- [7] R. J. Mailloux, *Phased Array Antenna Handbook*, 2nd ed. Norwood, MA: Artech House, 2005.
- [8] Y. L. Ban, C. Li, C. Y. D. Sim, G. Wu, and K. L. Wong, "4G/5G multiple antennas for future multi-mode smartphone applications," *IEEE Access*, vol. 4, pp. 2981-2988, 2016.
- [9] N. Ojaroudiparchin, M. Shen, S. Zhang, and G. F. Pedersen, "A switchable 3-D-coverage-phased array antenna package for 5G mobile terminals," *IEEE Antennas Wireless Propag. Lett.*, vol. 15, pp. 1747-1750, 2016.
- [10] J. Ala-Laurinaho, J. Aurinsalo, A. Karttunen, M. Kaunisto, A. Lamminen, J. Nurmiharju, A. V. Rasainen, J. Saily, and P. Wainio, "2-D beam-steerable integrated lens antenna system for 5G E-band access and backhaul," *IEEE Transactions Microw. Theory Tech.*, vol. 64, no. 7, pp. 2244-2255, Jul. 2016.
- [11] M. Khalily, R. Tafazolli, T. A. Rahman, and M. R. Kamarudin, "Design of phased arrays of series-fed patch antennas with reduced number of the controllers for 28-GHz mm-wave applications," *IEEE Antennas Wireless Propag. Lett.*, vol. 15, pp. 1305-1308, 2016.
- [12] S. Payami, M. Ghoraishi, and M. Dianati, "Hybrid beamforming for large antenna arrays with phase shifter selection," *IEEE Trans. Wireless Commun.*, vol. 15, no. 11, pp. 7258-7271, Nov. 2016.
- [13] Y. Gao, R. Ma, Y. Wang, Q. Zhang, and C. Parini, "Stacked patch antenna with dual-polarization and low mutual coupling for massive MIMO," *IEEE Trans. Antennas Propag.*, vol. 64, no. 10, pp. 4544-4549, Oct. 2016.
- [14] A. Dadgarpour, M. Sharifi Sorkherizi, A. A. Kishk, and T. A. Denidni, "Single-element antenna loaded with artificial mu-near-zero structure for 60 GHz MIMO applications," *IEEE Trans. Antennas Propag.*, vol. 64, no. 12, pp. 5012-5019, Dec. 2016.
- [15] G. Oliveri, M. Salucci, and A. Massa, "Synthesis of modular contiguously clustered linear arrays through a sparseness-regularized solver," *IEEE Trans. Antennas Propag.*, vol. 64, no. 10, pp. 4277-4287, Oct. 2016.
- [16] L. Lizzi, F. Viani, R. Azaro, and A. Massa, "A PSO-driven spline-based shaping approach for ultra-wideband (UWB) antenna synthesis," *IEEE Trans. Antennas Propag.*, vol. 56, no. 8, pp. 2613-2621, Aug. 2008.
- [17] L. Lizzi, R. Azaro, G. Oliveri, and A. Massa, "Printed UWB antenna operating over multiple mobile wireless standards," *IEEE Antennas Wireless Propag. Lett.*, vol. 10, pp. 1429-1432, 2011.
- [18] B. Avser, J. Pierro, and G. M. Rebeiz, "Random feeding networks for reducing the number of phase shifters in limited-scan arrays," *IEEE Trans. Antennas Propag.*, vol. 64, no. 11, pp. 4648-4658, Nov. 2016.
- [19] P. Rocca, R. J. Mailloux, and G. Toso, "GA-based optimization of irregular subarray layouts for wideband phased array design," *IEEE Antennas Wireless Propag. Lett.*, vol. 14, pp. 131-134, 2015.
- [20] P. Rocca, M. D'Urso, and L. Poli, "Advanced strategy for large antenna array design with subarray-only amplitude and phase control," *IEEE Antennas Wireless Propag. Lett.*, vol. 13, pp. 91-94, 2014.
- [21] K. Deb, M. Mohan, and S. Mishra, "A fast multi-objective evolutionary algorithm for finding well-spread Pareto-optimal solutions," *KangAL Report*, no. 2003002, pp. 1-18, Feb. 2003.
- [22] K. Deb, M. Mohan, and S. Mishra, "Evaluating the ϵ -domination based multi-objective evolutionary algorithm for a quick computation of Pareto-optimal solutions" *Evol. Computat.*, vol. 13, no. 4, pp. 501-525, 2005.
- [23] D. H. Wolpert and W. G. Macready, "No free lunch theorems for optimization," *IEEE Trans. Evol. Comput.*, vol. 1, no. 1, pp. 67-82, Apr. 1997.
- [24] P. Rocca, M. Benedetti, M. Donelli, D. Franceschini, and A. Massa, "Evolutionary optimization as applied to inverse problems," *Inverse Problems*, vol. 25, pp. 1-41, Dec. 2009.
- [25] R. L. Haupt and D. H. Werner, *Genetic algorithms in electromagnetics*. Hoboken, New Jersey: John Wiley and Sons, 2007.
- [26] R. L. Haupt, "Thinned arrays using genetic algorithms," *IEEE Trans. Antennas Propag.*, vol. 42, no. 7, pp. 993-999, Jul. 1994.
- [27] Federal Communications Commission, *Use of Spectrum Bands Above 24 GHz For Mobile Radio Services* [online], Sept. 2016. Available: https://apps.fcc.gov/edocs_public/attachmatch/FCC-16-89A1.pdf
- [28] International Telecommunication Union, *ITU towards "IMT for 2020 and beyond"* [online]. Available: <http://www.itu.int/en/ITU-R/study-groups/rsg5/rwp5d/imt-2020/Pages/default.aspx>
- [29] G. Oliveri and T. Moriyama, "Hybrid PSO-CP technique for the synthesis of non-uniform linear arrays with maximum directivity," *J. Electromagn. Wav. Appl.*, vol. 29, no. 1, pp. 113-123, Jan. 2015.
- [30] Z. Bayraktar, M. Komurcu, J. A. Bossard and D. H. Werner, "The wind driven optimization technique and its application in electromagnetics," *IEEE Trans. Antennas Propag.*, vol. 61, no. 5, pp. 2745-2757, May 2013.
- [31] M. D. Gregory, S. V. Martin and D. H. Werner, "Improved electromagnetics optimization: the covariance matrix adaptation evolutionary strategy," *IEEE Antennas Propag. Mag.*, vol. 57, no. 3, pp. 48-59, Jun. 2015.
- [32] O. Schutze, A. Lara and C. A. C. Coello, "On the influence of the number of objectives on the hardness of a Multiobjective Optimization problem," *IEEE Trans. Evol. Comput.*, vol. 15, no. 4, pp. 444-455, Aug. 2011.
- [33] D. Hadka *et al.*, *MOEA Framework (v. 2.9)* [online]. Available: <http://moeaframework.org>
- [34] C. A. Balanis, *Antenna Theory, Analysis and Design*, 2nd ed., New York: Wiley, 1997.